Figure 1

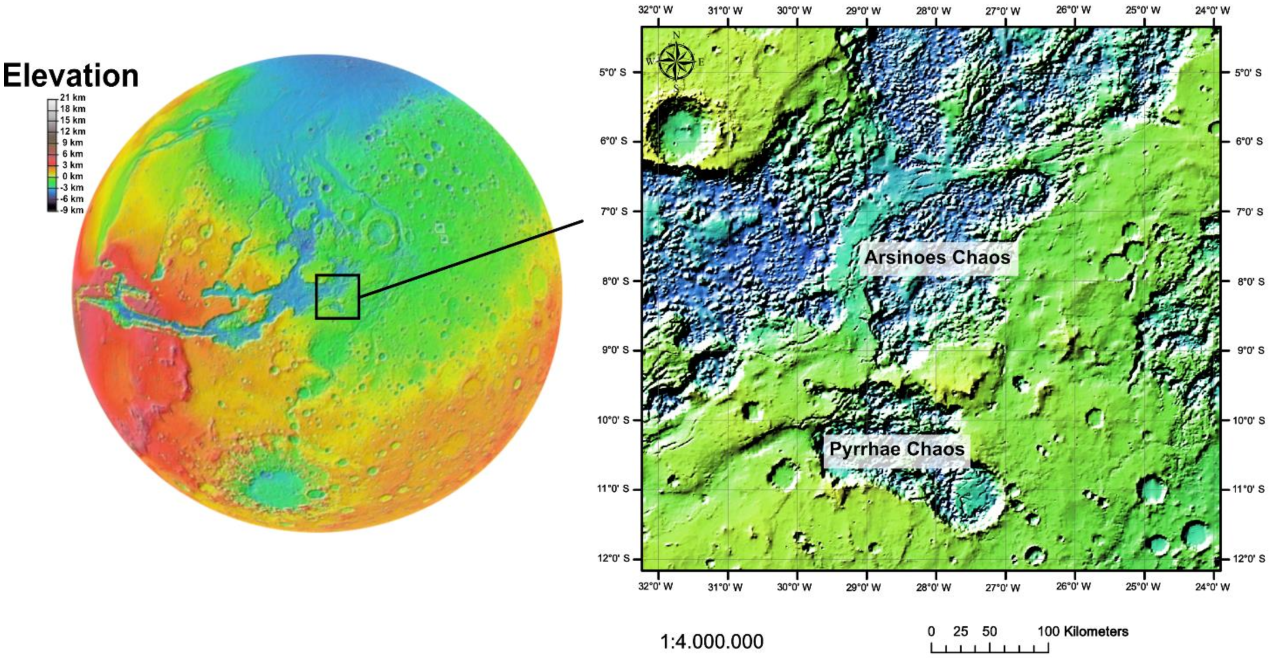

Elevation
21 km
18 km
15 km
12 km
9 km
6 km
3 km
0 km
-3 km
-6 km
-9 km
32°0' W
31°0' W
30°0' W
29°0' W
28°0' W
27°0' W
26°0' W
25°0' W
24°0' W
5°0' S
6°0' S
7°0' S
8°0' S
9°0' S
10°0' S
11°0' S
12°0' S
Arsinoes Chaos
Pyrrhae Chaos
1:4.000.000
0 25 50 100 Kilometers

Figure 2

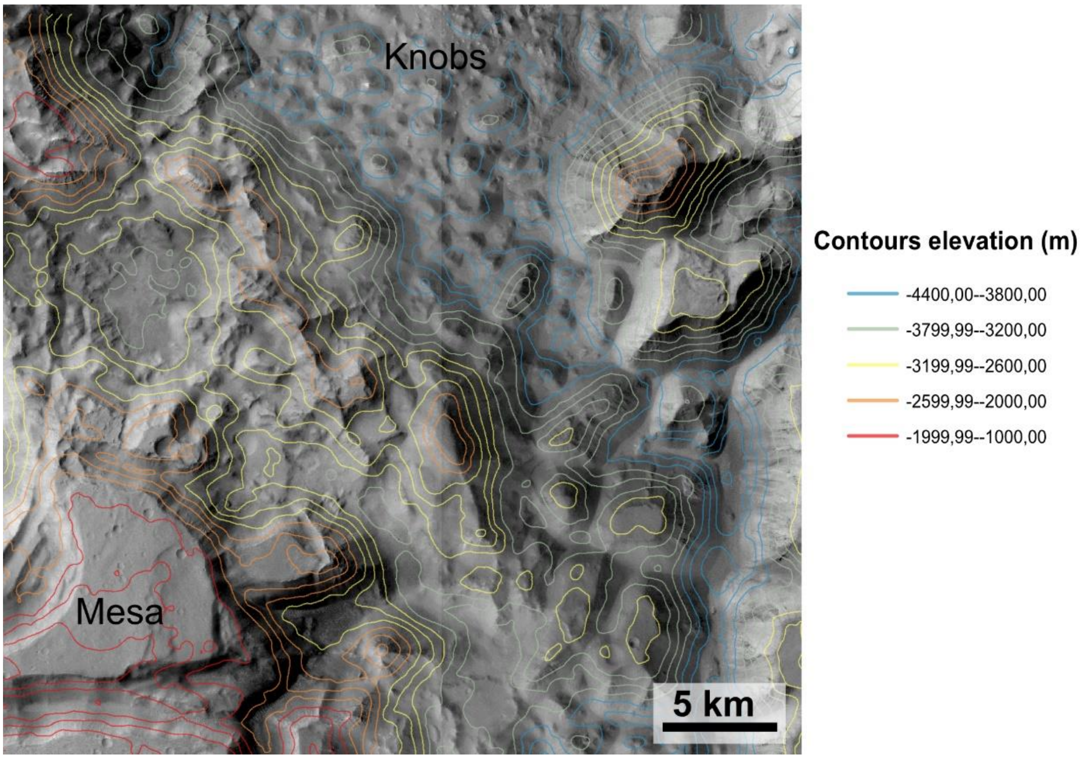
Knobs
Mesa
5 km
Contours elevation (m)
-4400,00--3800,00
-3799,99--3200,00
-3199,99--2600,00
-2599,99--2000,00
-1999,99--1000,00

Figure 3

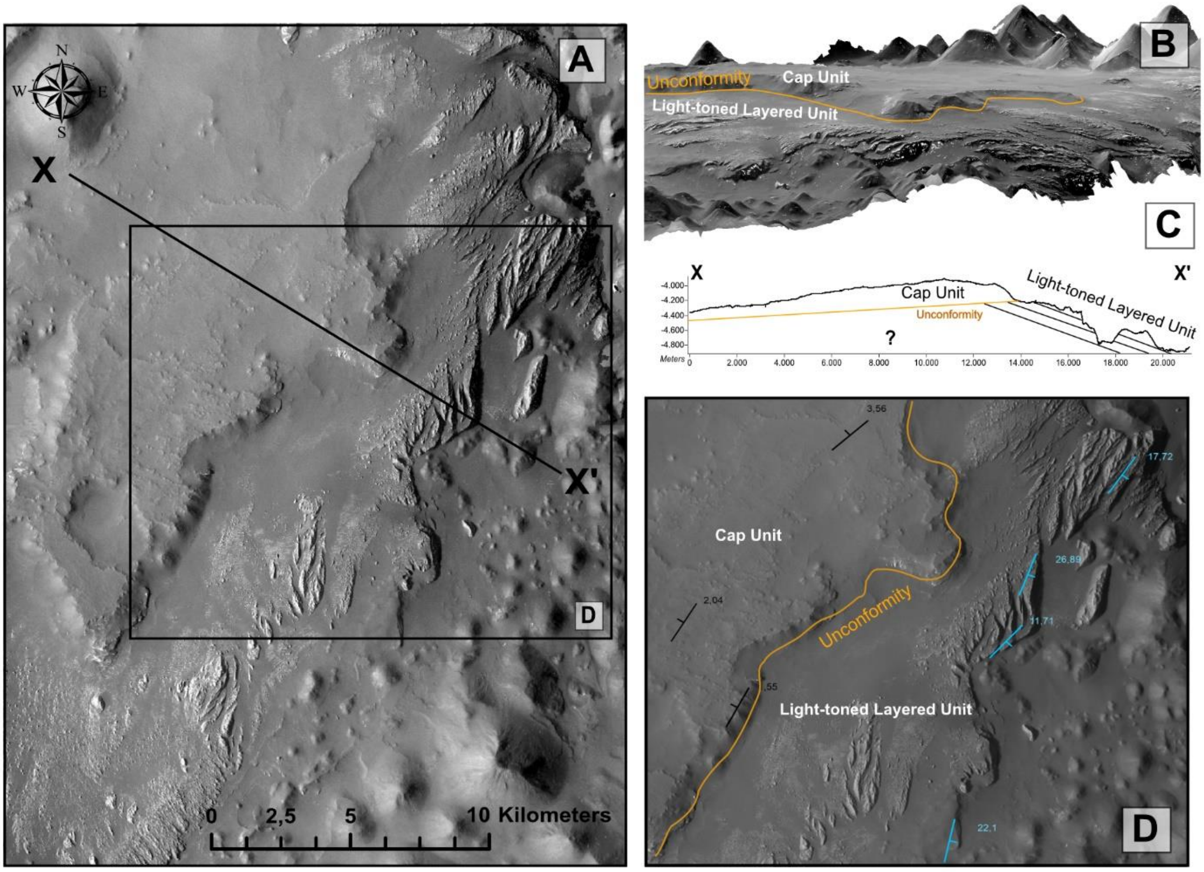
A
N
W
E
S
X
X'
D
0
2,5
5
10 Kilometers
B
Unconformity
Cap Unit
Light-toned Layered Unit
C
X
X'
Cap Unit
Light-toned Layered Unit
Unconformity
?
-4.000
-4.200
-4.400
-4.600
-4.800
Meters
0
2.000
4.000
6.000
8.000
10.000
12.000
14.000
16.000
18.000
20.000
3,56
17,72
Cap Unit
26,89
2,04
Unconformity
11,71
,55
Light-toned Layered Unit
22,1
D

Figure 4

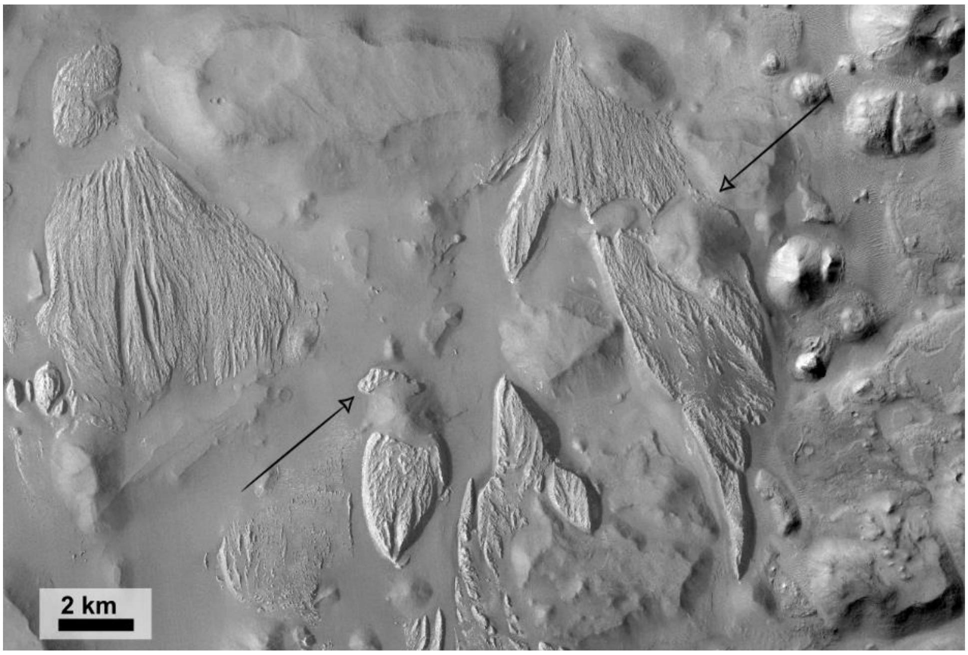

Figure 5

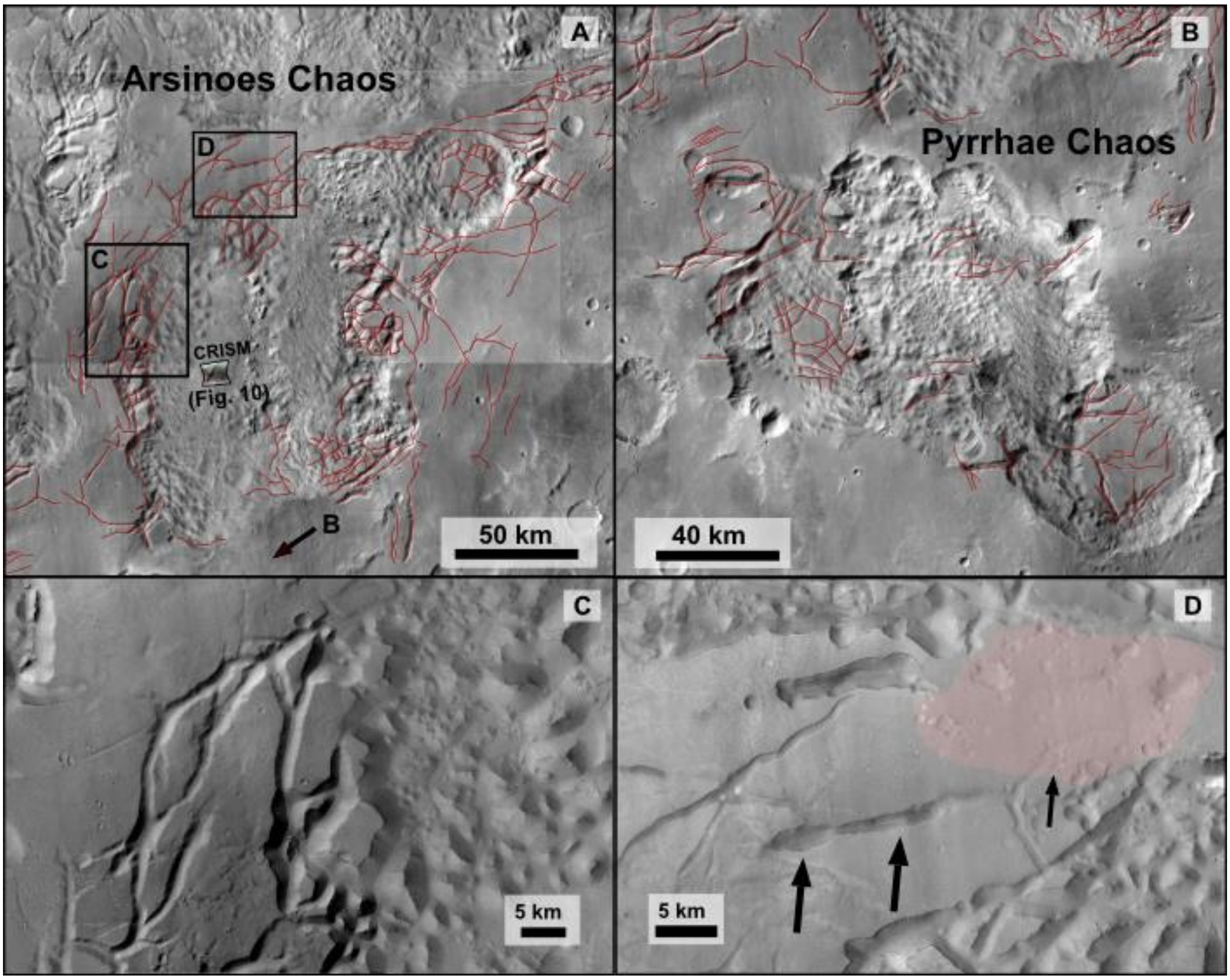

A
Arsinoes Chaos
D
C
CRISM
(Fig. 10)
B
50 km
B
Pyrrhae Chaos
40 km
C
5 km
D
5 km

Figure 6

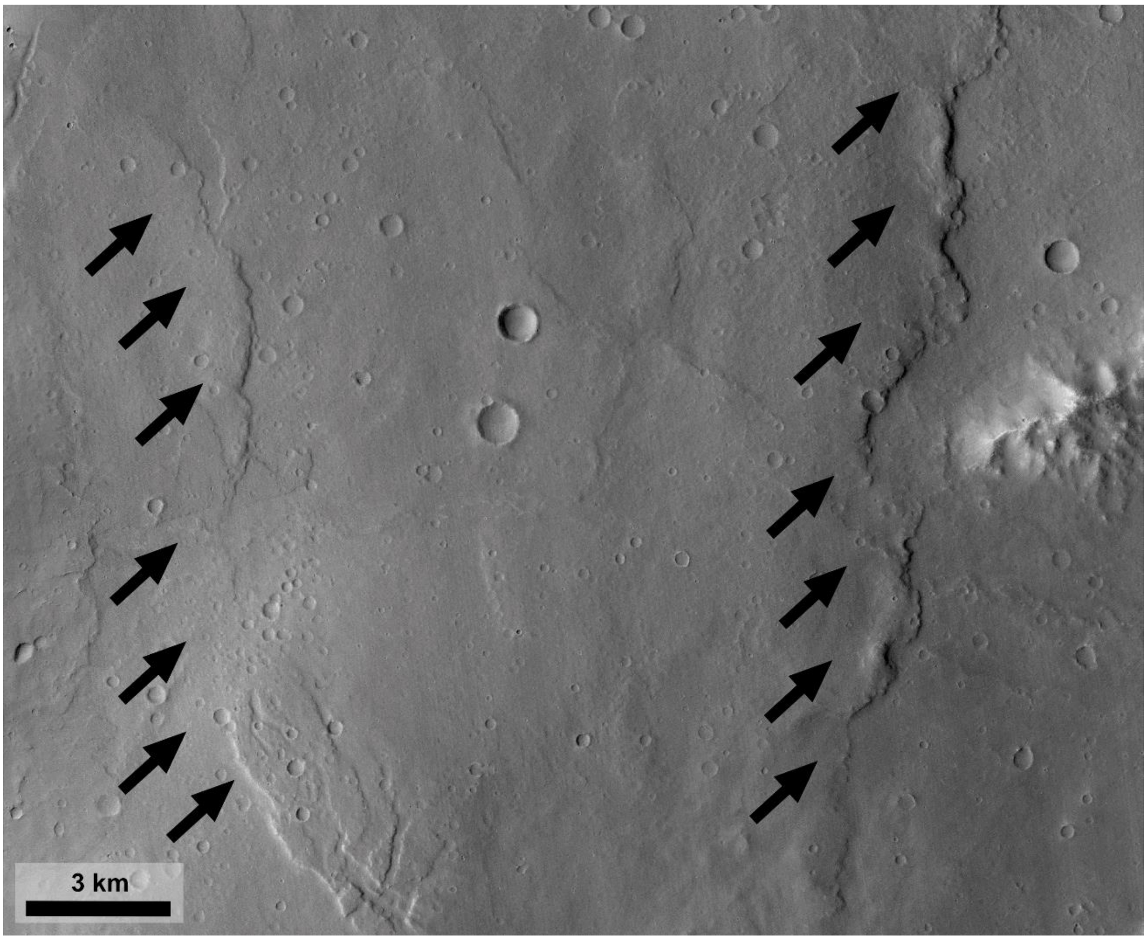

Figure 7

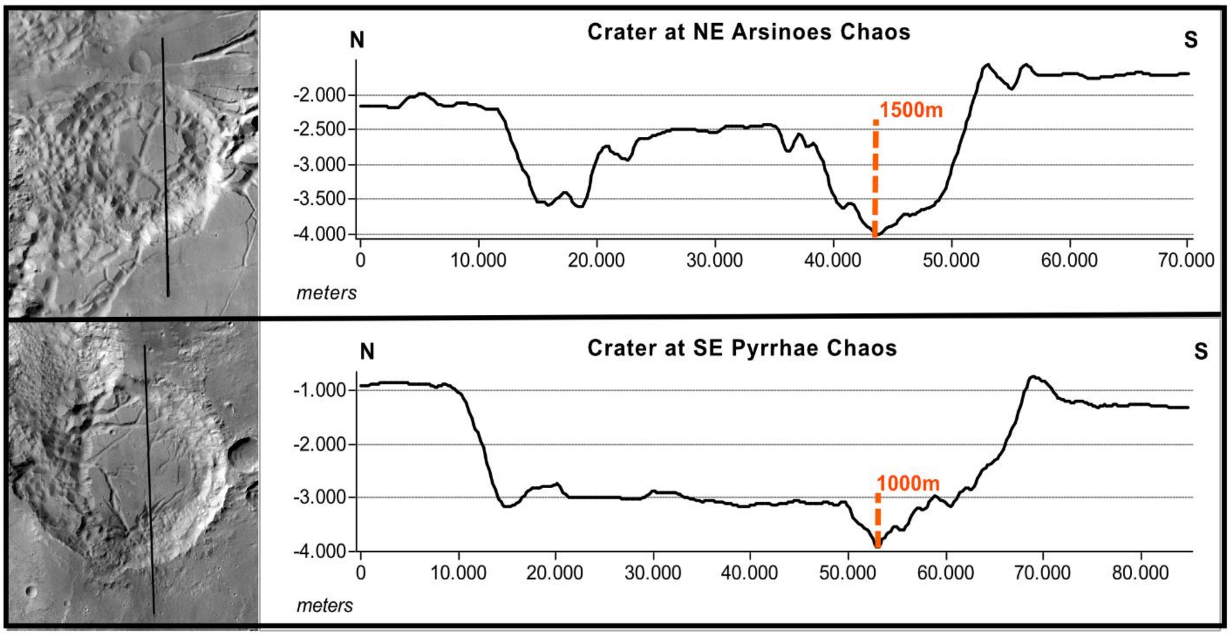

Crater at NE Arsinoes Chaos
N
S
1500m
-2.000
-2.500
-3.000
-3.500
-4.000
0
10.000
20.000
30.000
40.000
50.000
60.000
70.000
meters
Crater at SE Pyrrhae Chaos
N
S
1000m
-1.000
-2.000
-3.000
-4.000
0
10.000
20.000
30.000
40.000
50.000
60.000
70.000
80.000
meters

Figure 8

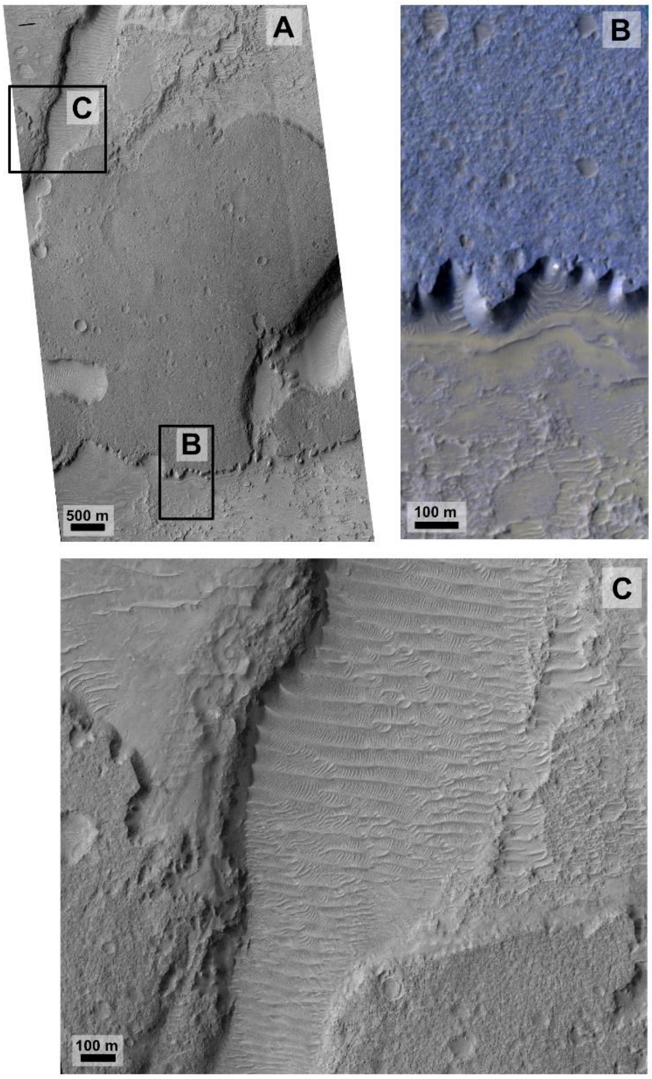

Figure 9

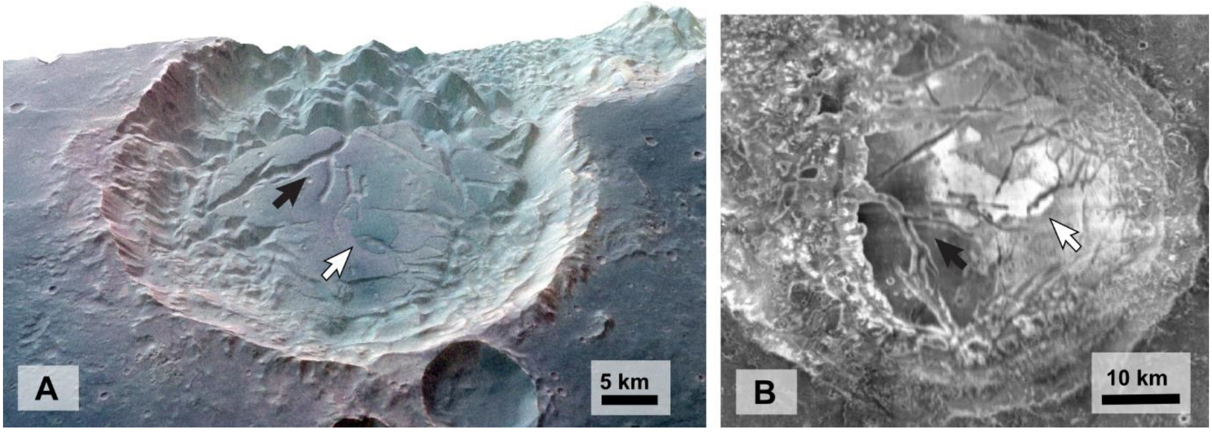

Figure 10

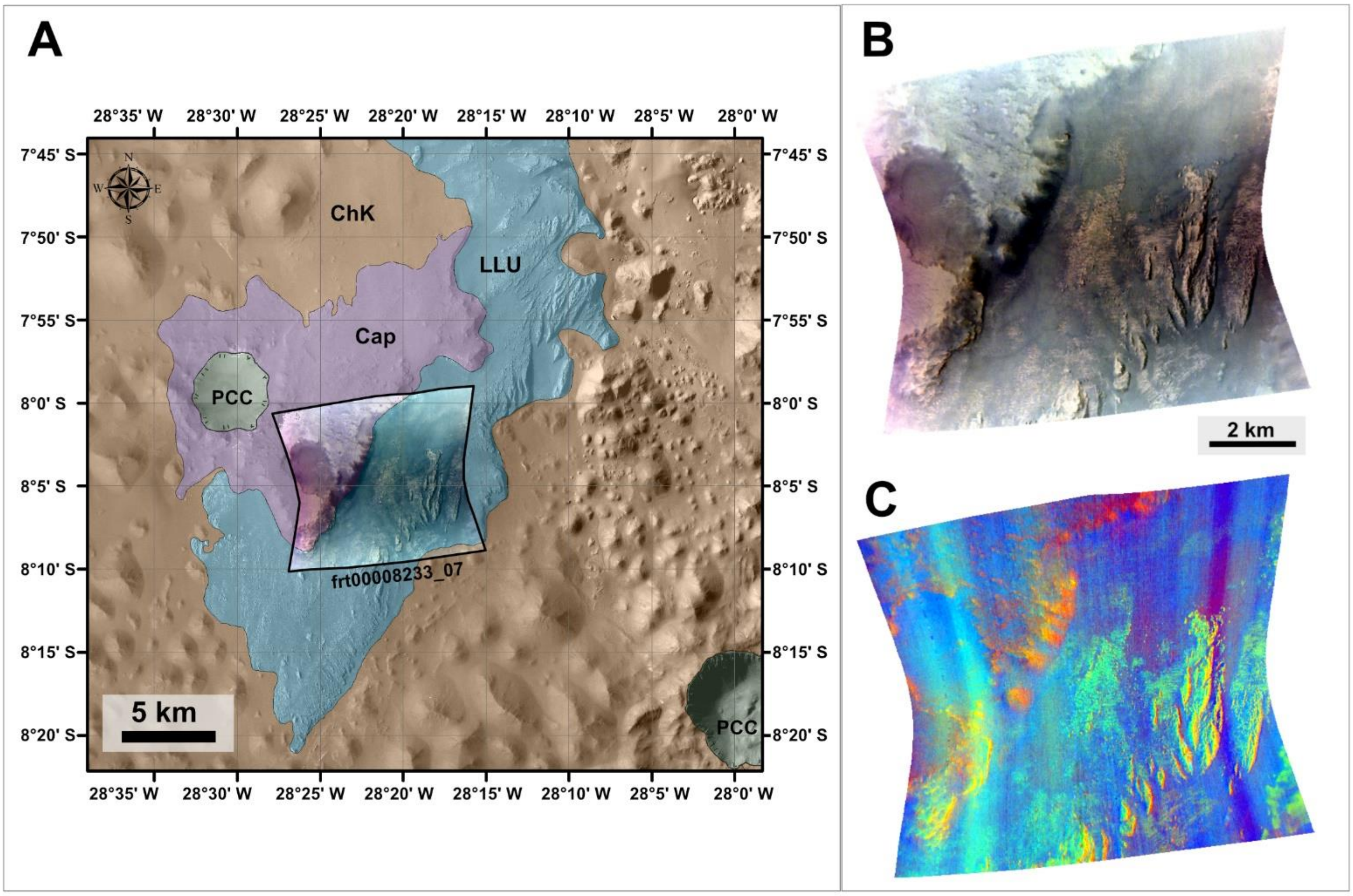
A
28°35' W
28°30' W
28°25' W
28°20' W
28°15' W
28°10' W
28°5' W
28°0' W
7°45' S
7°50' S
7°55' S
8°0' S
8°5' S
8°10' S
8°15' S
8°20' S
ChK
LLU
Cap
PCC
PCC
frt00008233_07
5 km
B
2 km
C

Figure 11

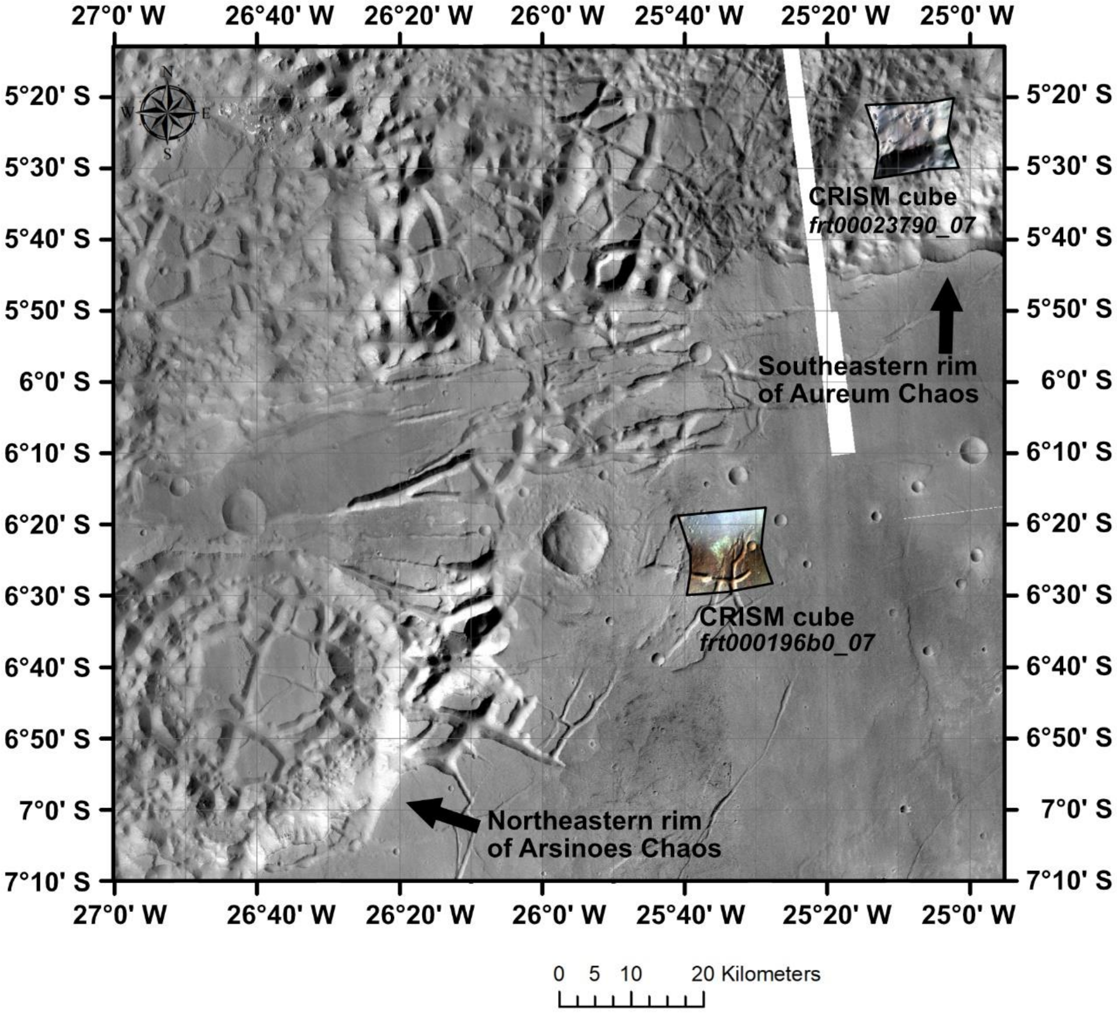
27°0' W
26°40' W
26°20' W
26°0' W
25°40' W
25°20' W
25°0' W
5°20' S
5°30' S
5°40' S
5°50' S
6°0' S
6°10' S
6°20' S
6°30' S
6°40' S
6°50' S
7°0' S
7°10' S
N
W
E
S
CRISM cube
frt00023790_07
Southeastern rim
of Aureum Chaos
CRISM cube
frt000196b0_07
Northeastern rim
of Arsinoes Chaos
0 5 10 20 Kilometers

Figure 12

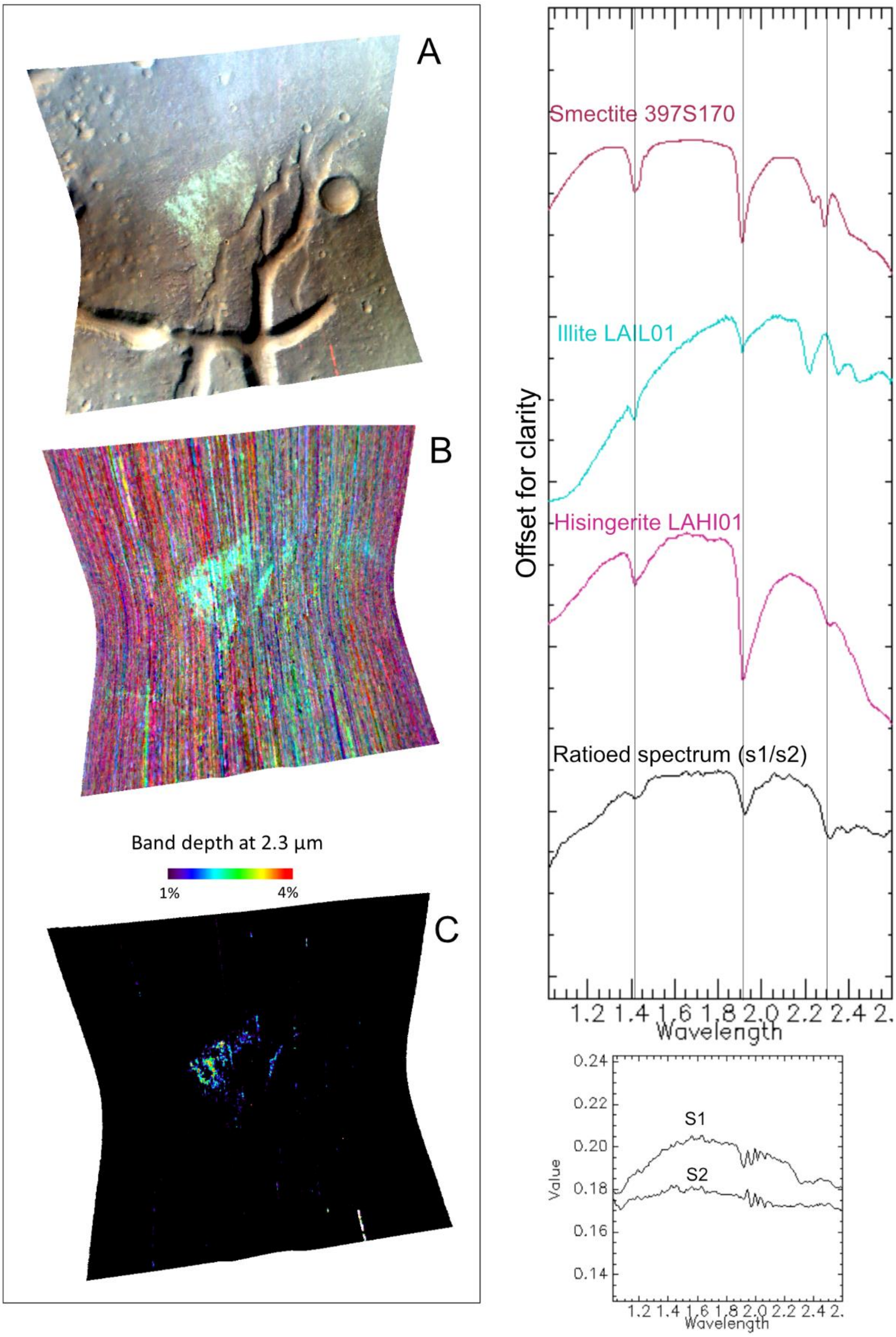

A
B
Band depth at 2.3 µm
1%
4%
C
Smectite 397S170
Illite LAIL01
Hisingerite LAHI01
Ratioed spectrum (s1/s2)
Offset for clarity
1.2 1.4 1.6 1.8 2.0 2.2 2.4 2.
Wavelength
0.24
0.22
0.20
0.18
0.16
0.14
Value
S1
S2
1.2 1.4 1.6 1.8 2.0 2.2 2.4 2.
Wavelength

Figure 13

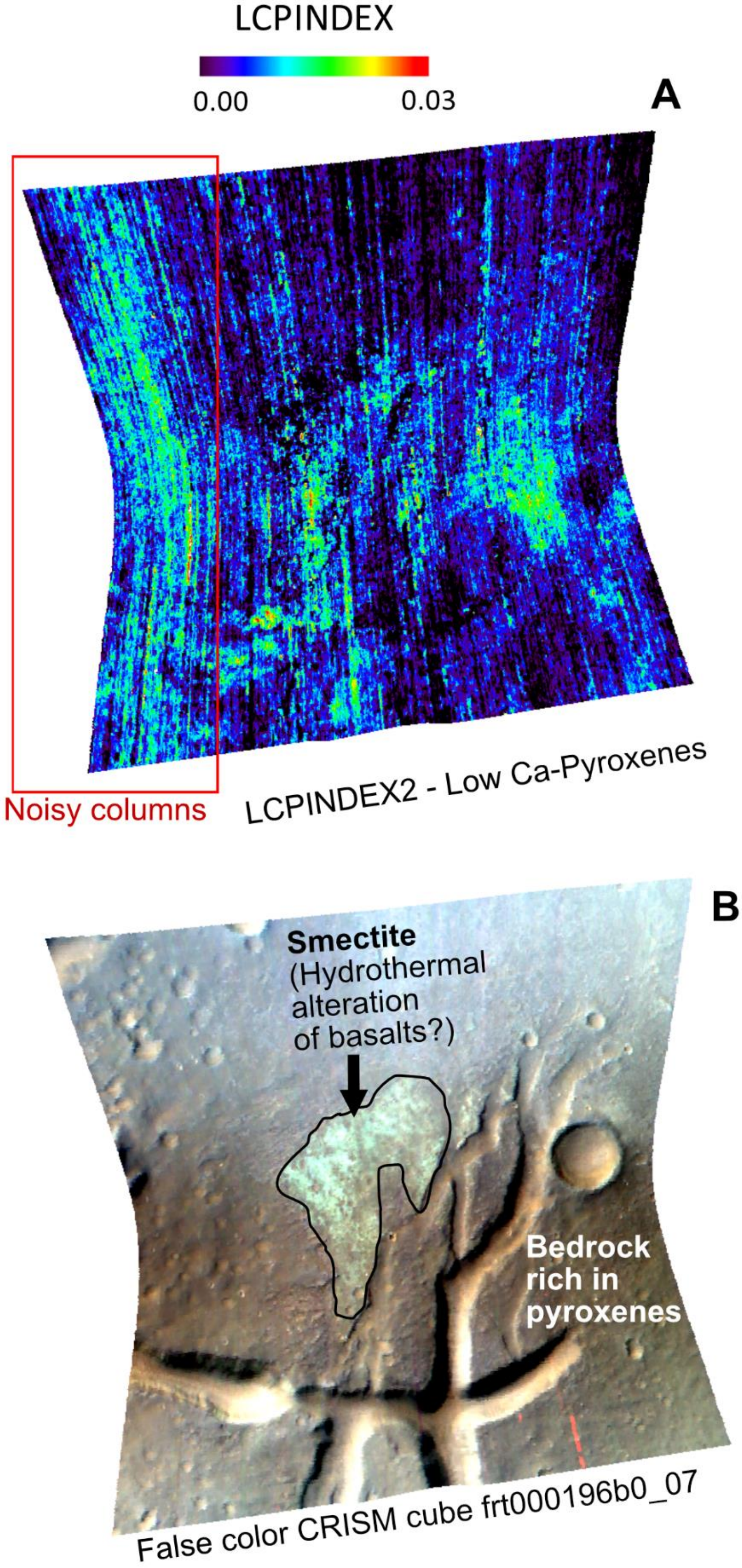
LCPINDEX
0.00
0.03
A
Noisy columns
LCPINDEX2 - Low Ca-Pyroxenes
B
Smectite
(Hydrothermal
alteration
of basalts?)
Bedrock
rich in
pyroxenes
False color CRISM cube frt000196b0_07

Figure 14

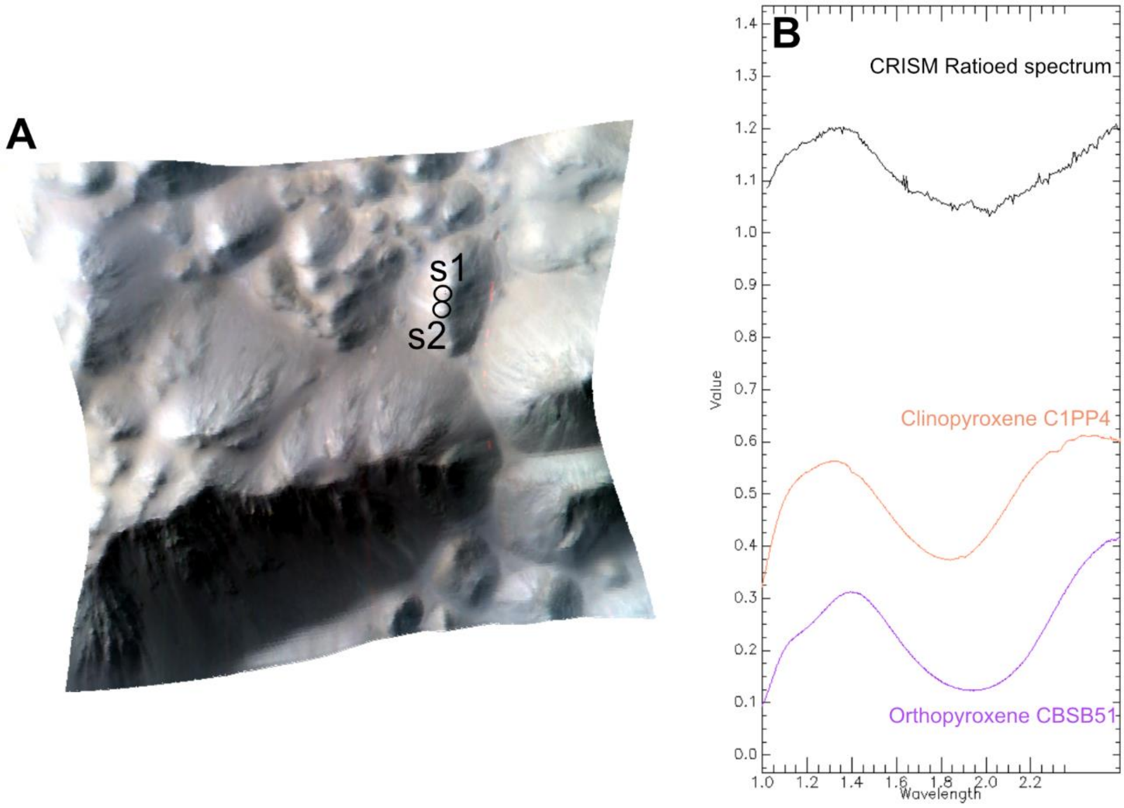
A
s1
s2
B
CRISM Ratioed spectrum
Clinopyroxene C1PP4
Orthopyroxene CBSB51
Value
Wavelength
1.4
1.3
1.2
1.1
1.0
0.9
0.8
0.7
0.6
0.5
0.4
0.3
0.2
0.1
0.0
1.0
1.2
1.4
1.6
1.8
2.0
2.2

Figure 15

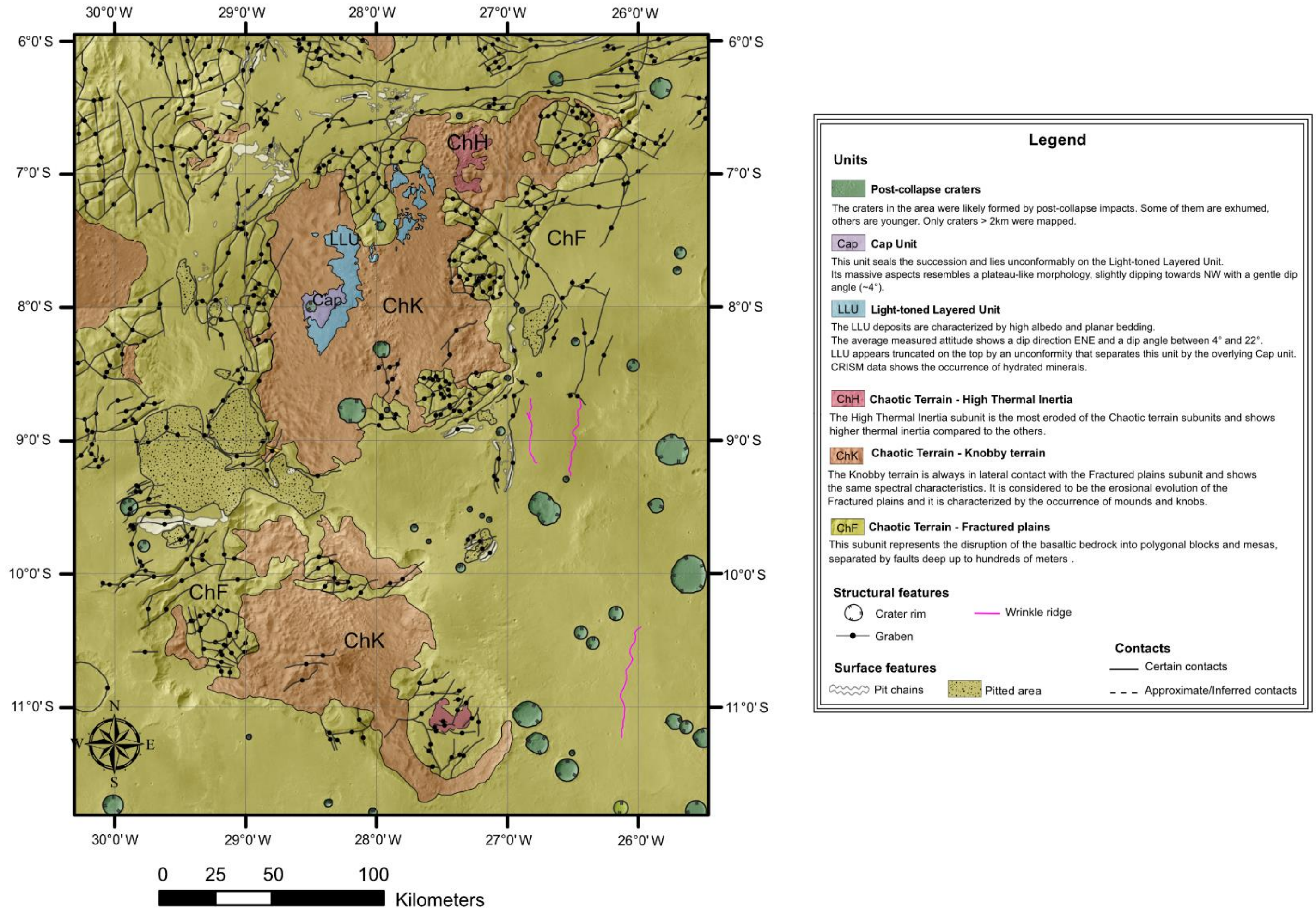

30°0' W
29°0' W
28°0' W
27°0' W
26°0' W
6°0' S
7°0' S
8°0' S
9°0' S
10°0' S
11°0' S
ChH
LLU
Cap
ChK
ChF
ChF
ChK
N
S
W
E
0 25 50 100
Kilometers
Legend
Units
Post-collapse craters
The craters in the area were likely formed by post-collapse impacts. Some of them are exhumed, others are younger. Only craters > 2km were mapped.
Cap
Cap Unit
This unit seals the succession and lies unconformably on the Light-toned Layered Unit.
Its massive aspects resembles a plateau-like morphology, slightly dipping towards NW with a gentle dip angle (~4°).
LLU
Light-toned Layered Unit
The LLU deposits are characterized by high albedo and planar bedding.
The average measured attitude shows a dip direction ENE and a dip angle between 4° and 22°.
LLU appears truncated on the top by an unconformity that separates this unit by the overlying Cap unit.
CRISM data shows the occurrence of hydrated minerals.
ChH
Chaotic Terrain - High Thermal Inertia
The High Thermal Inertia subunit is the most eroded of the Chaotic terrain subunits and shows higher thermal inertia compared to the others.
ChK
Chaotic Terrain - Knobby terrain
The Knobby terrain is always in lateral contact with the Fractured plains subunit and shows the same spectral characteristics. It is considered to be the erosional evolution of the Fractured plains and it is characterized by the occurrence of mounds and knobs.
ChF
Chaotic Terrain - Fractured plains
This subunit represents the disruption of the basaltic bedrock into polygonal blocks and mesas, separated by faults deep up to hundreds of meters .
Structural features
Crater rim
Wrinkle ridge
Graben
Surface features
Pit chains
Pitted area
Contacts
Certain contacts
Approximate/Inferred contacts

Tectono-magmatic, sedimentary and hydrothermal history of Arsinoes and Pyrrhae Chaos, Mars

Erica Luzzi[1], Angelo Pio Rossi[1], Cristian Carli[2] and Francesca Altieri[2]

[1]Jacobs University, Bremen, Germany
[2]Inaf-IAPS Tor Vergata, Rome, Italy
Corresponding author: Erica Luzzi (e-luzzi@jacobs-university.de)

Key points

- We produced a morpho-stratigraphic map of Arsinoes and Pyrrhae Chaos, including the volcanic grabens occurring throughout the study area;
- Spectral analyses of the light-toned deposits provide clues for sedimentary and hydrothermal minerals; spectral analyses of the bedrock are indicative of basaltic compositions;
- The observed volcano-tectonic surface features and the lack of evidences of any fluvial activity suggest that magmatic processes might be primarily responsible for the collapse of the chaotic terrain.

Abstract

Arsinoes and Pyrrhae Chaos are two adjacent chaotic terrains located east of Valles Marineris and west of Arabia Terra, on Mars. In this work we produced a morpho-stratigraphic map of the area, characterized by a volcanic bedrock disrupted into polygonal mesas and knobs (Chaotic Terrain Unit) and two non-disrupted units. The latter present a spectral variation, likely associated with hydrated minerals, and they are here interpreted as sedimentary units. The reconstructed geological history of the area starts with the emplacement of the basaltic bedrock, followed by the collapse that caused the formation of the chaotic terrains. Since evidences of volcano-tectonic activity are widespread across the area (e.g. fissure vents/graben, radial and concentric systems of faults, y-shaped conjunctions, lava flows, pit chains), and an intricate system of lava conduits is hypothesized for the occurrence of such features, we propose the possibility that the whole collapse was caused primarily by volcano-tectonic processes. In a late stage, after the end of the volcano-tectonic activity, a lacustrine/evaporitic depositional environment could have set, with the deposition of the non-disrupted units. The hydrated minerals found in the periphery of the Chaos could be the result of hydrothermal alteration of the basaltic bedrock.

Keywords:Chaotic terrains; Mapping; Spectral analyses; Mars; Hydrothermal system.

Plain Language Summary

Chaotic terrains are peculiar features on Mars. They consist of broad regions characterized by a variable surface disruption pattern of large polygonal blocks. Formation scenarios in the literature have always included a collapse, possibly caused by a range of processes, all including water or hydrated compounds (magma-ice interactions, melting of buried ice, groundwater pressure, etc.). In this work, we propose volcano-tectonic processes as mechanism of formation for closed chaotic terrains. Additionally, our mineralogical analyses suggest that during a late stage of the volcanic activity a hydrothermal system could have set. In such scenario hot water would have risen from the subsurface through fractures created by the volcanic activity, evolving from eruptive to hydrothermal. However, water would not have been directly involved in the initial collapse that formed the chaos.

1 Introduction

Arsinoes and Pyrrhae Chaos are two adjacent chaotic terrains, respectively centered at 7.8°S, 332°E and 10.3°S, 331.5°E (Fig. 1), a few tens of kilometres south of Aureum Chaos and a few hundred kilometres SW of Aram Chaos, sharing with the latter many structural and depositional characteristics. Several mechanisms of formation were proposed in literature to explain the nature of the putative collapse responsible for the disruption of the bedrock into polygonal blocks that characterizes the chaotic terrains. The proposed scenarios include: i) a major role played by groundwater and cryosphere, particularly linked to changes of pressure within the aquifer that caused the disruption of the bedrock and subsequent water outflow (Andrews-Hanna & Phillips, 2007; Carr, 1979; Harrison & Grimm, 2009; Rodriguez et al., 2005), ii) the occurrence of a buried ice lake that after melting would have caused fracturing and catastrophic outflow (Manker & Johnson, 1982; Roda *et a*l., 2014; Zegers *et al*., 2010), iii) catastrophic destabilization of buried clathrates (Hoffman, 2000; Kargel et al., 2007), and iv) magma-cryosphere/groundwater interactions (Chapman & Tanaka, 2002; Head & Wilson, 2007; Leask *et al*., 2006; Meresse et al., 2008; Wilson & Head III, 2002). Given the complexity of the current geologic setting of Arsinoes and Pyrrhae Chaos, possibly augmented by an extended time of erosion and mantling, a possible interaction between the proposed processes (or singular contributions at different times) must also be considered.

In the present work we performed the morpho-stratigraphic mapping of Arsinoes and Pyrrhae Chaos and a spectral analysis of the deposits. We propose a possible sequence of events to explain the occurrence of the collapsed bedrock involving magmatic processes followed by an aqueous depositional environment.

1.2 Regional setting

The first comprehensive description of chaotic terrains was made by Sharp et al. (1971) using Mariner 6 imagery, followed by Sharp (1973) based on Mariner 9 data and Schultz et al. (1982) based on Viking data. In this early stage of research, the main features of Martian chaotic terrains were already clear and these areas were defined as deeply collapsed terrains disrupted into an irregular pattern of tilted mesas and knobs, in some cases associated with outflow channels. The Chaotic Terrain Unit was first defined by Schultz and Rogers (1982) and then with a refinement by Glotch & Christensen (2005) into three subunits: Fractured Plains, Knobby Terrain and High Thermal Inertia Chaotic Terrain. The Chaotic Terrain Unit is interpreted as the basaltic bedrock (Christensen et al., 2000; Glotch & Christensen, 2005) and occurs over a large area including several other chaotic terrains such as Aureum, Aram, Hydratoes, Aurorae, Chryse and Hydaspis Chaos. The age of the Chaotic Terrain Unit according to Tanaka *et al.*, (2014) is Middle Noachian, with younger Hesperian ages in the internal portions of collapsed areas. With the collection of new compositional data from THEMIS (Thermal Emission Imaging System), TES (Thermal Emission Spectrometer), OMEGA (Observatoire pour la Minéralogie, l'Eau, les Glaces et l'Activité) and CRISM (Compact Reconnaissance Imaging Spectrometer for Mars), the investigations in literature focused mainly on the sedimentary units lying on top of the basaltic bedrock. Several authors analyzed the mineralogy of the layered sedimentary units occurring for example in Aram Chaos (Catling & Moore, 2003; Christensen *et al*., 2001; Dobrea *et al*., 2008; Gendrin *et al*., 2005; Glotch & Christensen, 2005; Lichtenberg *et al*., 2010; Liu *et al.*, 2012; Massé *et al.*, 2008; Ormö *et al*., 2004), Aureum and Iani Chaos (Dobrea *et al*., 2008; Glotch & Rogers, 2007; Sefton-Nash *et al*., 2012). Hematite deposits associated with monohydrated and polyhydrated sulfates were spatially correlated with layered sedimentary units, separated by an unconformity from the basaltic bedrock. The occurrence of hydrated sulfates and hematite allowed some authors to assume that an aqueous and/or hydrothermal depositional environment must have set after the collapse of the bedrock. The sedimentary layered deposits in Arsinoes Chaos were not included in the previous studies, while in Pyrrhae Chaos the sedimentary deposits are not observed at all. The lack of studies in this location emphasizes the need to expand our knowledge of this area, providing a broader context on Martian chaotic terrains.

2 Data and methods

2.1 Data, processing and tools

The imagery used to perform the geological mapping is provided by the CTX (Context Camera) (Malin *et al.*, 2007) and HiRISE (High Resolution Imaging Science Experiment) (McEwen *et al*., 2007) instruments onboard the MRO (Mars Reconnaissance Orbiter). One HRSC (High Resolution Stereo Camera, on board Mars Express spacecraft) image was also used to observe in false colour the study area and one HRSC DEM (Digital Elevation Model) was downloaded for the topographic contours in eastern Pyrrhae Chaos, since the area is not covered by CTX stereo pairs. CTX imagery was used as a basemap; in particular we used a global blended CTX mosaic provided by the Murray Lab (Dickson *et al*., 2018). HiRISE images were used to observe in detail the stratigraphic contacts in certain areas: EDR products were processed and tiled through the USGS software ISIS3 (Gaddis *et al.*, 1997). The data processing was supported by GNU Parallel (Tange, 2011). Variations in thermal inertia were investigated on JMARS (Java Mission-planning and Analysis for Remote Sensing) (Christensen *et al*., 2009) developed by ASU's Mars Space Flight Facility. JMARS is a Geographic Information System (GIS) where different layers can be loaded on a global basemap: it was used to visualize the THEMIS (Thermal Emission Imaging System) Derived Global Thermal Inertia Mosaic.

DEMs from CTX were computed using ASP (Ames Stereo Pipeline) developed by NASA (Beyer *et al.*, 2018; Moratto *et al*., 2010): the resulting products are bundle-adjusted to the global topography (MOLA - Mars Orbiter Laser Altimeter). A list of the used images is provided in Table 1.

The imagery was then imported into ESRI Arcgis for the geological mapping. The bedding attitudes were measured using the beta version of LayerTools (Kneissl *et al.*, 2011), kindly provided by Dr. Thomas Kneissl.

The CRISM (Murchie *et al.*, 2007) cubes (*S* detector - short wavelength channel, and *L* detector - long wavelength detector) with full resolution (FRT) available in the study area (also listed in Table 1) were processed by means of the software ENVI (with the CAT extension) where atmospheric corrections and projection were applied, allowing the subsequent visualization and analysis of the spectra.

2.2 Mapping

2.2.1 Scale

The geological map of the area was digitized on ArcGIS at the CTX resolution (~5 m/px), but the chosen output scale is 1:3.000.000.

Only craters with a diameter larger than 2 km were mapped.

2.2.2 Polygonal features – Morpho-stratigraphic units

The units observed in the study area are five and were mapped as polygons. The units include the three subunits of the Chaotic Terrain unit (*Fractured Plains, Knobby Terrain* and *High Thermal Inertia Chaotic Terrain*) and the non-disrupted units (*Light-toned Layered Unit* and *Cap unit*). Furthermore, the inner part of the post-collapse craters was mapped as an additional unit: *Post Collapse Craters*. Following the USGS guideline (2005), we chose warm colours for the Chaotic Terrain subunits given their volcanic nature. On the other hand, we chose to use cold colours for the non-disrupted units since they were interpreted as sedimentary deposits and green for the craters so that they could be clearly distinguished from the bedrock.

2.2.3 Linear features – Structural features and contacts

The mapped linear features include the crater rims, the contacts between different units and the structural features. The fractures affecting the bedrock and the elongated graben-like depressions were included in a single category called *grabens*. This choice is mainly due to the coalescence of the structures and the difficulty in distinguishing them. The second group of structural features is represented by the wrinkle ridges. The contacts were divided into *certain* contacts (continuous lines) and *approximate/inferred* contacts (dotted lines), for those cases where the mantling covers the contact (e.g. between Cap Unit and Light-toned Layered Unit) or if the change from one unit to another is transitional (e.g. between Knobby Terrain and High Thermal Inertia Chaotic Terrain).

2.2.4 Surface features – Pit chains and pitted areas

Pit chains and diffuse pits are widespread throughout the study area. In several parts the high density of pits did not allow to map individual pit chains, leading to the necessity to introduce a polygonal feature to indicate these areas (*Pitted areas*).

2.2.5 Symbols

The symbology used for crater rims, grabens, pit chains, wrinkle ridges, certain and approximate contacts was chosen in agreement with the standards recommended by USGS and FGDC for planetary mapping (FGDC, 2006). For pitted areas we introduced a new symbol.

3 Results

3.1 Morphological observations and stratigraphy

The stratigraphic relationships indicate that the oldest unit observed in Arsinoes and Pyrrhae Chaos is the Chaotic Terrain Unit, composed of three subunits: Fractured Plains (characterized by angular flat-topped blocks), the Knobby Terrain (displaying rounded mounds) and the High Thermal Inertia Chaotic Terrain (heavily eroded and characterised by the higher thermal inertia). The Fractured Plains occur predominantly along the rim of the Chaos, while the Knobby Terrain acts as a transition towards the inner parts of the Chaos. The Knobby Terrain subunit is the most extensive material representing the Chaotic Terrain Unit in this area. The Knobby Terrain is in contact with the sharp angular mesas of the Fractured Plains (Fig. 2) and the small mounds of the High Thermal Inertia Chaotic Terrain. The latter occurs only in a small area in the NE part of Arsinoes Chaos, in contact with the Knobby Terrain, and in a crater within Pyrrhae Chaos, in contact with the Fractured Plains. The rounded mounds characterizing the Knobby Terrain are located at lower elevations compared to the mesas of the Fractured Plains (Fig. 2). The scarps bounding the mesas of the Fractured Plains show a depth up to 1 km and the flat-topped blocks appear as irregular polygonal bodies. The mesas of the Fractured Plains subunit show a layering implying multiple depositional events, nevertheless it is difficult to follow the layers in lateral continuity on the adjacent mesas due to the different erosion and therefore we could not constrain with precision this bedding.

Stratigraphically above the Chaotic Terrain Unit, non-disrupted and layered deposits lie unconformably. In Arsinoes Chaos, the non-disrupted deposits overlying the Chaotic Terrain Unit displays two different morphologies and attitudes. Furthermore, they occur at different elevations showing their stratigraphic relationship. Therefore, they were considered as two distinct units, the Light-toned Layered Unit (LLU) and the Cap Unit (Cap) (Fig. 3). At lower elevations, the light-toned deposits are characterized by planar bedding and scalloped surfaces; their morphology resembles the ILDs (Interior Layered Deposits) described by Sowe *et al*. (2007), Le Deit *et al.* (2008) and Schmidt *et al*. (2018). The average attitude of the light-toned layered deposits is ~ S80E, 20°. The LLU outflanks the mounds of the Knobby Terrain (Fig.

4), assuming often a lobate shape and wrapping around the knobs. The overlying sedimentary deposits (Cap Unit) are separated from the LLU by an unconformity: the attitude of the youngest deposits (informally called Cap Unit due to the fact that these deposits “seal” the succession) is ~ N70W, 3°. The Cap Unit does not seem to be layered or if it is, the bedding is massive and the outcrop visible today represents only one thick bed with a plateau-like morphology. The occurrence of these two non-disrupted units only in some areas of the Chaos leads to the question of whether the current extent represents approximately the original extent or the erosion obliterated a large portion of the deposits that were originally covering the entire Chaos.

In Pyrrhae Chaos the non-disrupted sedimentary units are not present, although the two adjacent Chaos show a similar depth (in certain areas of Pyrrhae Chaos the depth is even higher than Arsinoes Chaos).

3.2 Structural observations

In Arsinoes and Pyrrhae Chaos, as well as in other chaotic terrains, the main structural feature is represented by the deep fractures bounding the polygonal blocks of the Fractured Plains. The fractures are open and show no displacement. Erosion and degradation might have enhanced the opening of these fractures after their formation. The minimum depth of the fractures can be assumed by the height of the mesa from the floor, and it is on the order of few hundred meters, up to 1 km. Additionally, the floor of the chaotic terrain accommodates the non-disrupted units, thus preventing the determination of the real depth of the blocks. The orientation of fractures bounding the blocks follows two trends that show variations throughout the chaos. The polygonal geometries are due to the irregularly orthogonal disposition of these two trends (Fig. 5a-b).

A large number of elongated grabens were mapped (Fig. 5a-b). These confined structures, that may resemble channels at a first glance, are often in coalescence with the orthogonal fractures of the polygonal mesas (Fig. 5c). In addition, grabens are also in coalescence with pit chains and/or occur in areas heavily pitted (Fig. 5d). Considering graben-like depressions and fractures as belonging to the same group of structures, two patterns can be distinguished based on their orientation: one group of structures seems to follow the rim of the Chaos, showing therefore a concentric pattern with respect to the rim of the basin; another group shows instead a radial pattern that was likely radiating from the center of the basin outwards but that is now only visible in proximity of the Chaos rim, due to dust cover and younger overlying units occurring within the basin. When these two sets cross each other, polygonal blocks are defined. The elongated graben-like depressions have a linear or slightly sinuous morphology and do not show any braided system nor meanders. The depth range is between 100 and 400 meters (up to 1000 if we consider those bounding the Chaos), while the length can reach up to 40 km. Moreover, several elongated graben-like depressions display y-shaped bifurcations.

Although the non-disrupted deposits do not have complete lateral continuity, no major faults affecting them were detected, not even at the HiRISE resolution. However, the lack of continuity of these deposits due to erosion means we cannot exclude the existence of younger faults affecting the layered deposits.

Compressive structures such as wrinkle ridges were also observed ~30 km SE from Arsinoes Chaos (Fig. 6), providing an important clue on the existence of a compressional regional stress prior the formation of the widespread grabens (east to Arsinoes Chaos a wrinkle ridge is cut by a graben). The wrinkle ridges show a typical orientation ~N-S and are characterized by sinuous/arcuate morphologies.

The last important structural observation concerns two major pre-collapse craters that were incorporated in the collapse, one in the north-eastern Arsinoes Chaos and one in the south-eastern Pyrrhae Chaos (depicted in Fig. 7). The craters are both filled by material affected by the grabens. The infilling has a maximum observable thickness of 1500 m in the crater located at NE Arsinoes Chaos, while the thickness in SE Pyrrhae Chaos reaches only 1000 m. The appearance of the infilling deposits seems to not differ from the surrounding basaltic bedrock, suggesting that the impacts predate not only the collapse, but also the last volcanic resurfacing events. The rims of the craters are partially degraded (in both craters, the southern rim is less degraded than the northern rim) and remnants of the ejecta are only visible in the southeastern crater. An exposed lava flow occurs in the crater at SE Pyrrhae (Fig. 8a). The lava flow is darker and less eroded than the surrounding bedrock, less covered by dunes and dust (Fig. 8B), and it is overlying all the volcanic deposits, suggesting that it may represent a late volcanic resurfacing event. This last resurfacing event is still predating the collapse as evidenced in Fig. 8C, where both the lava flow and the underlying rest of the bedrock are cut by a graben.

3.3 Thermal Inertia

The surface temperature of a given area depends on the properties of the exposed materials, but it is also affected by external factors such as dust covering and atmospheric pressure. Diurnal changes in temperature can be detected and described through the thermal inertia, a bulk property of materials defined by the relationship between thermal conductivity, density, and specific heat of the considered material. These properties are different for each material and some of the factors influencing the thermal behaviour are for example grain size, cementation, packaging of the grains and degree of exposure. Therefore, surfaces with different thermal inertia are most likely indicative of a change in composition and/or physical properties. A material with high thermal inertia is able to gather the heat and conduct it beneath the surface during the day, while during the night the stored heat is released through the surface (Mellon *et al*., 2000). In this way the surface appears cold during the day and warmer during the night. High thermal inertia is typical of consolidated/lithified materials, such as an exposed bedrock, lava flows, indurated and compact rocks; on the other hand unconsolidated sands and dust show a low thermal inertia (Fergason *et al*., 2006). On Mars, thermal information is provided by TES (Thermal Emission Spectrometer, see e.g. Jakosky *et al.*, 2000; Christensen *et al.*, 2001), on board Mars Global Surveyor, and THEMIS (Thermal Emission Imaging System, see e.g. Christensen *et al*., 2004), on board 2001 Mars Odyssey. We investigated the thermal inertia visualising the THEMIS-Derived Global Thermal Inertia Mosaic on JMars.

As anticipated in the previous sections, two areas with higher thermal inertia were detected in the study area. The first area occurs in Arsinoes Chaos and corresponds to the most eroded part of the Chaotic Terrain Unit that was identified as the High Thermal Inertia Chaotic Terrain subunit. The differentiation from the Knobby Terrain is transitional and delineating a sharp boundary was not trivial, but the high thermal inertia seems to coincide with the most eroded and peaked knobs. The second area is located in Pyrrhae Chaos and corresponds to the lava flow previously described (Fig. 9), located in proximity of a set of grabens. In this case the contrast is sharp and well-defined and the higher thermal inertia coincides perfectly with the lava flow that differently from the surrounding basaltic bedrock does not present neither mantling nor regolith (except for small dunes within the pits on the surface of the lava flow).

3.4 CRISM spectral analyses

In the nearby Aram Chaos, Glotch & Christensen (2005), detected mixtures of sulfates and phyllosilicates (associated with plagioclases and pyroxenes) in different percentage in all the non-disrupted units (Cap Unit and layered units), using the TES and THEMIS datasets. Part of the layered deposits was interpreted by the authors as hematite-bearing, while within other layered deposits the iron oxide was not found. Moreover, Lichtenberg *et al.* (2010) provided a stratigraphic and mineralogical characterization of the hydrated sulfates occurring in Aram Chaos, based on CRISM data. The authors identified two sedimentary units: the oldest consisting of monohydrated sulfates intercalated with ferric hydroxy-sulfate or nanophase ferric oxides and the youngest bearing polyhydrated sulfates and crystalline hematite. Monohydrated sulfates were detected by Lichtenberg *et al.* (2010) observing minor absorptions at 2.1 and 2.4 μm; ferric hydroxy-sulfate was interpreted through absorptions at 2.238 μm, associated with minor absorptions at 1.49, 1.82, and 2.38 μm; polyhydrated sulfates were inferred from the absorptions at 1.9 and 2.4 μm within the youngest unit unconformably lying on the oldest with monohydrated sulfates. Polyhydrated sulfates in association with crystalline gray hematite have been found also by Dobrea *et al*. (2008) in Aram, Aureum and Iani Chaos: using the TES and OMEGA datasets, the authors were able to point out a correlation between all these chaotic terrains East of Valles Marineris. Sowe *et al.* (2012) analysed CRISM spectra from Aureum Chaos, and also in this case the authors were able to identify within the light-toned layered units hydroxylated, monohydrated, polyhydrated sulfates. The hydroxylated sulfates were interpreted by the authors based on the absorptions at 2.23 μm (related to the occurrence of OH), 1.42–1.45 μm and its weak 1.93 and 2.4 μm bands. Monohydrated sulfates (kieserite) were detected through absorptions at 2.12 μm and a major absorption at 2.4 μm, while polyhydrated sulfates were diagnosed based on absorptions at 1.42–1.44 and at 1.92–1.93 μm.

Considering these evidences from the nearby Aram and Aureum Chaos and given the morphologic analogies, we investigate if similar mineralogies can be detected also in Arsinoes Chaos.

Only one full resolution CRISM cube is available within the inner region of Arsinoes Chaos (*frt00008233_07_if164*). This cube was analysed in order to characterize the non-disrupted units overlying the basaltic bedrock. A first distinction of spectrally different terrains was made based on the RGB images (Fig. 10) with combined summary products (Viviano-Beck *et al.*, 2014). First, we examined the minerals revealed by previous works on chaotic terrains. In Fig. 10C the summary parameter for chlorides shows a possible occurrence of hydrated minerals (in yellow). The putative hydrated minerals coincide in extent with the morphologically identified Light-toned Layered Unit. The RGB composites derived from the parameters that are specifically used to identify hydrated minerals (such as sulfates and phyllosilicates) did not provide a clear distinction of a mineralogical variation. Moreover, the difficulty in finding a spectrum with clear evidences of hydrated minerals is attributed to the detection limit and to the noise affecting the data. Therefore, summary products suggest a mineralogical variation and likely bearing hydrated minerals, but the spectra do not allow the detection of specific minerals. The interpretation of these deposits as sedimentary can only be supported by analogies with the adjacent chaotic terrains and by the morpho-stratigraphic observations.

Other hydrated minerals (CRISM cube *frt000196b0_07*) were found in the northeastern periphery of Arsinoes Chaos (Fig. 11), within a deposit in correspondence of some of the collapse features previously described. Slightly north of this area we performed also analyses on the bedrock (CRISM cube *frt00023790_07* and *frt000196b0_07*).

The hydrated minerals detected in the CRISM cube *frt000196b0_07* are concentrated in the central area of the cube, precisely coinciding in extent with an exhumed deposit slightly different in albedo from the surrounding materials. As shown in Fig. 12A, a mineralogical variation is already distinguishable from the infrared false color image where the hydrated minerals appear to be pale green. This first clue is therefore additionally supported by the RGB composites in Fig. 12B and 12C. In 12B the RGB composite PFM is shown for the detection of Fe and Mg in the crystalline structure of the hydrated phyllosilicates, in particular for significant band depths at 2.3 μm; as a result, Fe-Mg hydrated phyllosilicates are displayed as cyan, allowing to appreciate the mineralogical variation at a first glance. For the ratioed spectrum the numerator is an average of some of the cyan pixels shown in Fig. 12B having both band depth at 1.9 and 2.3 micron well above the detection limit, while the denominator is an average of pixels with relatively flat spectra picked from the same column of their respective numerators. The resulting ratioed spectrum is reported in Fig. 12, where a comparison with spectra from the CRISM resampled library is provided. Several phyllosilicates sharing similar absorptions (indicative of Fe, Mg-OH) were plotted in order to compare even the weakest absorption to understand the corresponding mineral that may occur in the deposit. We interpreted the ratioed spectrum as smectite, since the ratioed spectrum and the smectite's spectrum share the same absorptions, including the absorption at 2.28 μm that is instead shifted toward > 2.3 μm in the other plotted phyllosilicates, due to a bigger concentration of Fe instead of Mg (Clark *et al.*, 1990).

On the same CRISM cube *frt000196b0_07* analyses of the bedrock revealed the occurrence of mafic minerals, in particular pyroxenes with low Ca content. A first identification of the pyroxenes was made by analyzing the summary product LCPINDEX2 (low-Ca pyroxenes) (Fig. 13). A significant spectrum for the analysis of the bedrock results from the CRISM cube *frt00023790_07*, where broad absorptions at 1 μm and 2 μm confirm the occurrence of pyroxenes (Fig. 14) (Viviano-Beck *et al*., 2014). The asymmetry of the absorption at 1 μm towards longer wavelength could also be associated with the occurrence of a second mafic phase as olivine or an high-Ca pyroxene, with variations in breadth due to the amount of Fe and Mg or Ca (Cloutis *et al*., 1986; King & Ridley, 1987). Pyroxenes and olivine are indicative of basaltic compositions. This observation supports the basaltic nature of the bedrock of the chaotic terrain (Chaotic Terrain Unit).

3.5 Morpho-stratigraphic map

The observations carried on and described in the previous section led to the creation of a morpho-stratigraphic map of the area (Fig. 15).

The units were classified through photo-interpretation, taking into consideration: visible and sharp contacts, transitional contacts, differences in texture, degree of erosion and mantling, morphology, bedding when occurring, relative relationships between units, attitudes and compositional information where available. The bedrock of the area is identified in the Chaotic Terrain Unit, a basaltic unit subdivided into three subunits: the Chaotic Terrain Fractured Plains (ChF on the map), the Knobby Chaotic Terrain (ChK) and the High Thermal Inertia Chaotic Terrain (ChH). Because of the volcanic nature of the Chaotic Terrain Unit, the three subunits were mapped with warm colors. An unconformity separates the bedrock from the overlying Light-toned Layered Unit (LLU), while a second unconformity is interposed between the LLU and the overlying Cap Unit (Cap) that seals the succession. Spectral data showed the possibility that LLU is composed by hydrated minerals, but the detection limit and the low quality of the

CRISM cube did not allow a specific classification of the hydrated minerals. On the other hand, hydrated minerals classified as Fe- and Mg-phyllosilicates were found in a small deposit in the northeastern periphery of Arsinoes Chaos, but the limited extent did not allow to represent it on our map at this scale.

Craters in the area with a diameter larger than 2 km were mapped as Post-collapse crater.

As for the other features (pit chains, wrinkle ridges, grabens, and crater rims), they were mapped using the standard symbols FGDC. We introduced a new symbol for pitted areas, where the pits were highly coalescent and concentrated making it difficult to map the single feature.

The produced map contributes to fill the gaps regarding Chaotic terrains, but most importantly it highlights the need to expand the availability of maps in this complex area in order to facilitate future works and discussions.

4 Discussion

4.1 Pre-collapse events and Floor-Fractured craters

The information that we gathered on the pre-collapse stratigraphy is limited to a few observations: i) the basaltic mesas of the Chaotic Terrain Unit present different layers, suggesting multiple volcanic resurfacing events before the collapse; ii) the ancient impact craters occurring in NE Arsinoes Chaos and SE Pyrrhae Chaos predate the collapse since they are filled with materials affected by the collapse-related structures; iii) it is still unclear if the three subunits of the Chaotic Terrain Unit represent just a different lateral erosional evolution of the same material or if the different erosional patterns are due to a lateral mineralogical variations as yet undetected. The craters in NE Arsinoes Chaos and SE Pyrrhae Chaos were likely formed between the multiple eruptive events that emplaced the Chaotic Terrain Unit and afterwards they have been embedded into the collapse. The crater in NE Arsinoes Chaos, presents a thicker infilling, a more eroded rim and no sign of ejecta: these could be clues of an older age compared to the crater in SE Pyrrhae Chaos that has a thinner infilling and visible traces of the eroded ejecta. We have to keep in mind that both of them are filled by fractured materials; therefore, even though the southeastern crater may be younger, it still predates the collapse and the end of the lava supply that formed the Chaotic Terrain Unit.

This particular type of craters affected by polygonal fractures were classified on Mars by Bamberg et al. (2014) as FFCs (Floor-Fractured Craters). FFCs have been extensively studied on the Moon: the origin of their fractures was attributed to two main processes. One of the discussed processes is the viscous relaxation of the crater topography proposed by Hall et al. (1981) but then proved wrong by Dombard & Gillis (2001); the other proposed process (the most widely accepted) consists of a sill emplacement and consequent inflation (Jozwiak et al., 2015; Jozwiak et al., 2012; Thorey & Michaut, 2014; Wichman & Schultz, 1996). Bamberg et al. (2014) performed an accurate global classification of the martian FFCs, dividing them into two groups: one group of FFCs occur in fluvial areas and were formed (or modified after the formation) by fluvial activity. The second group (that includes our area of study) was attributed to intrusive volcanism: the factors considered by the authors include absence of fluvial morphologies and outflow channels, but also occurrence of volcanic pits, collapsed lava conduits, lava sheets, and basaltic composition of the bedrock. We agree with this interpretation and we propose that processes related to magmatic intrusion could explain on a large scale the collapse of the chaotic terrain itself in absence of aqueous-related surface features.

4.2 Bedrock collapse

The widespread occurrence of grabens leads to question their nature and the possibility that they could be linked to the origin of the collapse. Following Scott & Wilson (2002), grabens are interpreted here as volcanic graben. Similar structures within the Tharsis region, on Olympus Mons and Ascraeus Mons, were interpreted as fissure vents by Mouginis-Mark & Christensen (2005), but also as fluvial-related by Scott & Wilson (1999). Furthermore, grabens similar to that occurring in Arsinoes and Pyrrhae Chaos were mapped and interpreted as vents in Ascraeus Mons (Mars) by Pozzobon *et al.* (2015). Such vents would have erupted lavas coming from a complex network of dykes, while collapsed pits would be associated with feeder dykes. Dykes were invoked for the formation of grabens and pit chains also in Pavonis Mons by Montési (2001), where the author describes the possible interactions between dykes and volatiles and the resulting structures based on the degree of interaction. According to Montési (2001), grabens are formed by deep dykes that do not reach the volatile-rich layer but stop at the extensional stage; if the dyke is able to quickly reach the volatile-rich layer, their interaction results into pits; coalescing pit chains would be formed by an intermediate interaction between the dyke and the volatile-rich layer.

In first instance, we rule out the possibility that the grabens may have any connection with fluvial systems: no braided nor meandering patterns were recognized, as well as no tributaries nor typical fluvial depositional morphologies anywhere in the study area. Since outflow channels or other fluvial features are lacking, a volcano-tectonic origin seems more likely, considering the basaltic mineralogies across the area, the presence of y-shaped conjunctions indicative of inflation and at least one evident lava flow spatially associated with the fissures (Fig. 8A). Moreover, the grabens have a significant depth (up to 1000 m), that could be explained by a constant flow (in case of water) and not by a periodic/stagnant river;

nevertheless there are no evidences of such a developed hydrographic system, and the channels terminate abruptly without fluvial deposits nor confluence into other channels. Additionally we rule out that grabens were formed by groundwater sapping which, as evidenced by Lamb et al. (2006) is unlikely to erode in short time a basaltic bedrock (and if it spanned over a long period then we would expect more hydrated alteration of the basalts). Irwin et al. (2014) performed remote sensing analyses on the valleys within the desert of Atacama and discussed the possibility to infer if groundwater sapping caused the incision of the valleys on Mars or not. The authors argue that theater-headed valleys on Mars should not be interpreted as due to groundwater sapping by default because many other factors may influence the formation of the headscarps, and the morphology of the valleys *per sē* cannot justify such interpretation.

According to Mège & Masson (1996), the grabens occurring in Valles Marineris were formed during Hesperian as a passive rift system, but the authors do not exclude the possibility of an interplay with magmatic processes related to the Tharsis region that occurred in a more recent span of time. Tanaka & Golombek (1989) propose that tension fractures were responsible for the formation of grabens on Mars, particularly in the area of Valles Marineris. These authors argue that the orientations of grabens and pit chains suggest a structural control that cannot be attributed to volcanic processes since no volcanic deposits occur in correspondence of these structures. Nevertheless, more recent works (with access to younger and better datasets than in 1989) showed the occurrence of widespread basaltic mineralogies within the chaotic terrains (Glotch & Christensen, 2005), small pitted cones interpreted as of volcanic nature (Meresse et al., 2008), dykes within Valles Marineris (Flahaut et al., 2011; Mège & Gurgurewicz, 2016; Okubo & Schultz, 2005) and lava flows draping the outflow channels (Leone, 2014).

Therefore, based on the mentioned references and on our observations, the grabens that we described and interpreted as volcanic grabens (*sensu* Scott & Wilson, 2002) may be considered as the result of the collapse of lava conduits, or fissure vents, or due to inflation processes originated from buried magma chambers and/or buried magma intrusions, or as due to the ascent of dykes.

Another surface evidence for such collapses is represented by the extensive pits and pit chains, that at a first glance may resemble small craters but lack in ejecta and raised rims. Pits and pit chains were interpreted in literature as the surface collapse of buried lava conduits (Leone, 2014), as collapse due to magma stoping or as the result of explosive activity, likely due to interactions between magma and H_2O (Head & Wilson, 2002; Okubo & Martel, 2005; Wyrick, 2004), and as the result of the interaction between dykes and volatiles (Montési, 2001). An additional interpretation based on a terrestrial analogue was proposed by Ferrill *et al.* (2011), who observed pit chains in Iceland formed by the interplay of dilational faults, extension fractures, and tectonic caves. The authors suggested a similar combination of mechanisms for the formation of pit chains on Mars. In our study area, extensional faults with clear displacements were not found, the polygonal blocks are different from the horst and graben systems on Earth because arranged in radial and concentric patterns. The pits and pit chains are often coalescent with volcanic grabens, suggesting perhaps extremely unstable conditions of interconnected plumbing systems. Moreover, pit chains that are often coalescent and intersect each other with different orientations suggest excluding a pure tectonic control.

An important topic that we want to mention is the origin of the outflow channels, absent in Arsinoes and Pyrrhae Chaos but occurring in association with other chaotic terrains. Despite the broad consensus of the scientific community on aqueous erosional processes carving the outflow channels (Andrews-Hanna & Phillips, 2007; Baker, 2001; Carr, 1979; Harrison & Grimm, 2008; Hoke *et al*., 2011; Leask *et a*l., 2007; Meresse *et al*., 2008; Rodriguez *et al*., 2005; Rodriguez *et al*., 2015), recently several authors proposed that the outflow channels might have been carved by lava flows (Jaeger et al., 2010; Leone, 2014; Leverington, 2011). Leverington (2011) lists and discusses the evidence against an aqueous origin of outflow channels: i) lack of fluvial deposits along the channels, together with deltas and sedimentary shoreline features, while channels seem to be lava draped instead; ii) incompatibility between the amount of required water and the global mineralogical observations of the unaltered olivine; iii) paucity of analogues in the solar system of large-sized channels carved by aquifer outburst; iv) the required permeability of the megaregolith might not be realistic. In contrast with the aqueous origin of outflow channels the author highlights how a volcanic origin seems to be the simplest explanation based on the evidences on the martian surface.

Koeppen & Hamilton (2008) performed a global analysis of the olivine end-member mineralogies found on the martian surface: they postulated that the poor alteration of the olivine could be interpreted as due to spatially inhomogeneous wet conditions in the early climate, with very wide dry areas, or to the short-term availability of water on Mars.

Based on our overall observations in our area of study, we speculate that it would be possible that the trigger of the outflow channels could have been magmatic bodies heating the permafrost. The absence of outflow channels in our area of study could be explained by a lateral variation of the permafrost thickness and/or possibly the local fracturing state of the uppermost crust.

Reassessing the extent of the role played by water or lava in forming outflow channels is beyond the aim of this work. The literature reviewed above follows two schools of thought, but we believe that both water and magmatic processes contributed to the final geological setting of chaotic terrains, one prevailing on the other and vice versa at different times.

We observed hydrated mineralogies, especially in the periphery of Arsinoes Chaos, while in the inner Chaos the detection of hydrated minerals is weaker and limited to the RGB composites. The spectra there did not allow the identification of specific phases, probably because their abundance is below the detection limit. Therefore, we confirm that water was present but our interpretation, based on the stratigraphic relationships between the observed geological units and structures, separate the major contributions of volcanic and aqueous processes in two stages: during the first stage, magmatic processes were mainly responsible for the collapse of the chaotic terrain, possibly interacting with volatiles and/or permafrost; in a second stage (post-collapse) water played a major role (perhaps for a short time given the limited extent of the hydrated deposits).

4.3 Thermal Inertia

The high thermal inertia of the lava flow occurring in Pyrrhae Chaos could be related to the younger age of the lava flow than the surrounding bedrock. A high thermal inertia is normally observed in lava flows, but the absence of high thermal inertia in the underlying basaltic bedrock (except for the most eroded subunit, the High Thermal Inertia Chaotic Terrain, and for the steep slopes of the mesas, recognizing that mantling debris on slopes may thermally obscure to different extents) is due to the fact that the Chaotic Terrain unit is partially covered by regolith and/or mantling. Our guess is that the basaltic bedrock underlying the lava flow could be older than the overlying lava flow, and therefore more affected by mantling and weathering, while the lava flow is still acting thermally as a rocky surface. The interplay between dust cover and thermal behaviour has been already investigated on Mars by Crown & Ramsey (2017), based on a THEMIS IR survey in Arsia Mons. These authors describe the difficulties in discriminating the effect of mantling and albedo from the real thermal inertia, but they were able to identify two types of lava flow: one group with relatively high albedo and large extent and a second one darker, smooth and smaller, associated with elongated channels and fissures, very similar to the lava flow observed in Pyrrhae Chaos.

Despite the inferred younger age of the lava flow with respect to the surrounding basaltic bedrock, we found that the lava flow predates the collapse since it is cut by a volcanic graben. Thus, the lava flow could be interpreted as the last recognizable volcanic resurfacing event, probably toward the end of the hypothesized multi-phase volcanic activity. The end of lava supply could have been responsible for the collapse of the plumbing system generating the volcanic grabens.

4.4 Non-disrupted units

The Light-toned Layered Unit and the Cap Unit were interpreted as sedimentary deposits first of all by analogy with the nearby chaotic terrains, where deposits sharing the same characteristics of those in Arsinoes Chaos were already interpreted as sedimentary units and spectral analyses were already carried out (Dobrea *et al*., 2008; Glotch *et al*., 2005; Glotch & Christensen, 2005; Glotch & Rogers, 2007; Lichtenberg *et al*., 2010; Sowe *et al*., 2012). Furthermore, we interpreted the non-disrupted units as sedimentary for the following reasons: Lack of volcano-tectonic features, high albedo, planar bedding, more prone to erosion than the surrounding basalts, and mineralogical variation that could be associated with occurrence of hydrated minerals

The reason why the NIR absorption features are not as prominent as in other CRISM data from Aureum and Aram Chaos may be due to several factors: a lower abundance of hydrated minerals, absence of areas bereft of hydrated minerals within the CRISM cube (thus the denominator cannot be ideal), lack of totally dust-free areas, features below the detection limit. Especially for the Cap Unit, it was not possible to determine from a compositional point of view the presence of the hydrated silicates detected in other similar sedimentary units because even in the RGB with combined summary products, no significant variation was appreciable.

Nevertheless, the observed variation in the Light-toned Layered Unit could be consistent with the interpretation of the layered deposits in the adjacent chaotic terrains, except for the high concentration of hematite that was well described in Aram and Aureum Chaos but was not found in Arsinoes Chaos. The hematite in Aram Chaos is considered by Glotch & Christensen (2005) as a fundamental key for a lacustrine interpretation together with the bedding and the closed geometry of the basin and the outflow channels. Despite the lack of hematite (missing or simply below the detection limit) and outflow channels in Arsinoes Chaos, the hypothesis of a lake or evaporitic basin as a depositional environment for the Light-toned Layered Unit cannot be excluded either. We consider reasonable that a closed and deep basin such as Arsinoes Chaos, that seems to possibly host hydrated minerals, might have been filled by groundwater after the collapse.

It remains uncertain why in Pyrrhae Chaos the sequence ends with the Chaotic Terrain Unit. The depth of the basin is approximately the same as Arsinoes Chaos (even deeper) and their proximity would suggest that the same processes should have acted, but for some reason the deposition of sedimentary units after the collapse did not happen in Pyrrhae Chaos (or the deposits were completely eroded).

The exhumed light-toned deposit found in the north-eastern periphery of Arsinoes Chaos were instead interpreted as related to hydrothermal activity that could have started as soon as the volcanic activity responsible for the collapse has begun to stabilize. This hypothesis is supported by the evidence of smectite within the deposit. In this case, the hydrated minerals are not in a closed basin, but associated with the volcano-tectonic structures that we interpreted as directly related to volcanic collapses. Furthermore, the associations of basaltic minerals (pyroxenes) and hydrated Fe-Mg phyllosilicates (smectite) can be explained by a process of hydrothermal alteration, as summarized by Inoue (1995). According to that author, smectite can be the result of hydrothermal alteration of andesitic to basaltic compositions under neutral or alkaline conditions.

On Earth, this has been observed in several geological contexts, including stagnant hydrothermal alteration of caldera deposits (Inoue *et al*., 1984). The extent of the hydrothermal deposit is limited to 1.3 km and for scale reasons it was not possible to include it in the geomorphic map. Nevertheless, in the surrounding area light-toned exhumed patches are visible, suggesting an extent of the hydrothermal deposit of at least 10 km.

5 Conclusion

The morpho-stratigraphic mapping performed in Arsinoes Chaos highlighted the occurrence of two major groups of geomorphic units: the basaltic Chaotic Terrain Unit, further subdivided into three subunits (Fractured Plain, Knobby Terrain and High Thermal Inertia Chaotic Terrain) represents the bedrock of the area and it is characterized by polygonal irregular mesas and rounded knobs; the second group is composed by two non-disrupted units (Light-toned Layered Unit and Cap Unit) that were deposited after the collapse of the Chaotic Terrain and lie unconformably on top of the bedrock.

The Light-toned Layered Unit is characterized by a planar bedding and the scalloped surfaces show high albedo; the Cap Unit seems instead to be a single thick layer (plateau-like) and lies unconformably on top of the Light-toned Layered Unit. In Pyrrhae Chaos the non-disrupted units are missing.

The spectral analyses performed in Arsinoes Chaos could not entirely confirm the morpho-stratigraphic evidences for the sedimentary deposits with the presence of hydrated phase similar to the case of Aram and Aureum lying on the bedrock of the Chaotic Terrain Unit. Nevertheless, a mineralogical variation is present and the existence of hydrated minerals below CRISM detection limits cannot be ruled out.

The bedrock was confirmed to be basaltic in composition due to the occurrence of mafic minerals, in particular low-Ca pyroxenes; the CRISM analyses did not reveal crucial information on the Cap Unit and Light-toned Layered Unit, but we detected hydrated minerals hosted by a small deposit located in proximity of the collapse-related structure in the northeastern periphery of Arsinoes Chaos and we identified hydrated Fe-Mg phyllosilicates (likely smectite). While the Light-toned Layered Unit may be explained by a lacustrine/evaporitic environment that could have been established after the collapse and the stabilization of the volcanic activity, the hydrated minerals occurring in the northeastern periphery cannot be explained by such a hypothesis because they are not placed into a closed basin, but they drape the volcano-tectonic structures interpreted as volcanic graben. For this reason, the most likely hypothesis involves a hydrothermal system where hot water rises through the fractures, deposits hydrated minerals and alters the pre-existing basaltic bedrock. The structural evidences of volcano-tectonic activity support this interpretation, suggesting that after the collapse the volcanic activity may have turned into a hydrothermal environment warming up the groundwater that was infiltrating the fractures and finally reaching the surface with processes of deposition and alteration. Given the lack of evidence for aqueous activity pre- and syn-collapse, and the occurrence of widespread volcanic features, we infer the collapse to have been triggered primarily by volcano-tectonic processes, possibly interacting with volatiles and/or permafrost. Further studies will reinforce or rule out this hypothesis.

6 Acknowledgments

We acknowledge support and funding from the European Union's Horizon 2020 research and innovation programme under grant agreement Nº776276 (PLANMAP). We are grateful to the reviewers and editors for their helpful comments. We also want to express our appreciation for the insights and the fruitful discussions with Dr. Riccardo Pozzobon.

The processed CRISM cubes and the geopackage of the morpho-stratigraphic map, including vectors and the raster of the basemap was stored in a repository following the FAIR principles (Luzzi et al., 2020). The CTX mosaic is described by Dickson *et al*. (2018) and since it is a beta version it does not have a DOI yet. A grid shapefile with the tiles and corresponding links can be downloaded at http://murray-lab.caltech.edu/CTX/tiles/beta01/Murray-Lab_CTX-Mosaic_beta01_QuadMap.zip. Alternatively the single CTX images can be downloaded at https://ode.rsl.wustl.edu/mars/indexproductsearch.aspx after setting the adequate parameters (MRO, CTX, Arsinoes Chaos, Pyrrhae Chaos). The HiRISE dataset is included in McEwen et al. (2007). The HRSC dataset is included in Walter & van Gasselt (2014).

7 References

Alexis, J., Rodriguez, P., Kargel, J. S., Baker, V. R., Gulick, V. C., Berman, D. C., … Glines, N. (2015). Martian outflow channels: How did their source aquifers form, and why did they drain so rapidly? OPEN. *Nature Publishing Group*. https://doi.org/10.1038/srep13404

Andrews-Hanna, J. C., & Phillips, R. J. (2007). Hydrological modeling of outflow channels and chaos regions on Mars. *Journal of Geophysical Research: Planets*, *112*(E8).

Baker, V. R. (2001). Water and the Martian landscape. *Nature*, *412*(6843), 228.

Bamberg, M., Jaumann, R., Asche, H., Kneissl, T., & Michael, G. G. (2014). Floor-fractured craters on mars - Observations and origin. *Planetary and Space Science*, *98*, 146–162. https://doi.org/10.1016/j.pss.2013.09.017

Beyer, R. A., Alexandrov, O., & McMichael, S. (2018). The Ames Stereo Pipeline: NASA's Open Source Software for Deriving and Processing Terrain Data. *Earth and Space Science*, *5*(9), 537–548. https://doi.org/10.1029/2018EA000409

Carr, M. H. (1979). Formation of Martian flood features by release of water from confined aquifers. *Journal of Geophysical Research*, *84*(B6), 2995. https://doi.org/10.1029/JB084iB06p02995

Catling, D. C., & Moore, J. M. (2003). The nature of coarse-grained crystalline hematite and its implications for the early environment of Mars. *Icarus*, *165*(2), 277–300. https://doi.org/10.1016/S0019-1035(03)00173-8

Chapman, M. G., & Tanaka, K. L. (2002). Related magma--ice interactions: Possible origins of chasmata, chaos, and surface materials in Xanthe, Margaritifer, and Meridiani Terrae, Mars. *Icarus*, *155*(2), 324–339.

Christensen, P. R., Engle, E., Anwar, S., Dickenshied, S., Noss, D., Gorelick, N., & Weiss-Malik, M. (2009). JMARS - A Planetary GIS. *American Geophysical Union, Fall Meeting 2009, Abstract Id.IN22A-06*. Retrieved from http://adsabs.harvard.edu/abs/2009AGUFMIN22A..06C

Christensen, P. R., Morris, R. V., Lane, M. D., Bandfield, J. L., & Malin, M. C. (2001). Global mapping of Martian hematite mineral deposits: Remnants of water-driven processes on early

Mars. *Journal of Geophysical Research: Planets*, *106*(E10), 23873–23885. https://doi.org/10.1029/2000JE001415

Christensen, P R, Bandfield, J. L., Hamilton, V. E., Ruff, S. W., Kieffer, • H H, Titus, T. N., … Greenfield, M. (2001). Mars Global Surveyor Thermal Emission Spectrometer experiment: Investigation description and surface science results. In *JOURNAL OF GEOPHYSICAL RESEARCH* (Vol. 106). https://doi.org/10.1029/2000JE001370

Christensen, Philip R., Bandfield, J. L., Smith, M. D., Hamilton, V. E., & Clark, R. N. (2000). Identification of a basaltic component on the Martian surface from Thermal Emission Spectrometer data. *Journal of Geophysical Research: Planets*, *105*(E4), 9609–9621. https://doi.org/10.1029/1999JE001127@10.1002/(ISSN)2169-9100.MGSTES1

Christensen, Philip R., Jakosky, B. M., Kieffer, H. H., Malin, M. C., McSween, Jr., H. Y., Nealson, K., … Ravine, M. (2004). The Thermal Emission Imaging System (THEMIS) for the Mars 2001 Odyssey Mission. *Space Science Reviews*, *110*(1/2), 85–130. https://doi.org/10.1023/B:SPAC.0000021008.16305.94

Clark, R. N., King, T. V. V., Klejwa, M., Swayze, G. A., & Vergo, N. (1990). High spectral resolution reflectance spectroscopy of minerals. *Journal of Geophysical Research*, *95*(B8). https://doi.org/10.1029/jb095ib08p12653

Cloutis, E. A., Gaffey, M. J., Jackowski, T. L., & Reed, K. L. (1986). Calibrations of phase abundance, composition, and particle size distribution for olivine-orthopyroxene mixtures from reflectance spectra. *Journal of Geophysical Research*, *91*(B11), 11641. https://doi.org/10.1029/jb091ib11p11641

Crown, D. A., & Ramsey, M. S. (2017). Morphologic and thermophysical characteristics of lava flows southwest of Arsia Mons, Mars. *Journal of Volcanology and Geothermal Research*, *342*, 13–28. https://doi.org/10.1016/J.JVOLGEORES.2016.07.008

Dickson, J., Kerber, L., Fassett, C., & Ehlmann, B. (2018). A Global, Blended CTX Mosaic of Mars With Vectorized Seam Mapping: A New Mosaicking Pipeline Using Principles of Non-Destructive Image Editing. *Lunar and Planetary Science Conference*.

Dobrea, E. Z. N., Poulet, F., & Malin, M. C. (2008). Correlations between hematite and sulfates in the chaotic terrain east of Valles Marineris. *Icarus*, *193*(2), 516–534.

Dombard, A. J., & Gillis, J. J. (2001). Testing the viability of topographic relaxation as a mechanism for the formation of lunar floor-fractured craters. *Journal of Geophysical Research: Planets*, *106*(E11), 27901–27909. https://doi.org/10.1029/2000JE001388

Fergason, R. L., Christensen, P. R., & Kieffer, H. H. (2006). *High-resolution thermal inertia derived from the Thermal Emission Imaging System (THEMIS): Thermal model and applications*. https://doi.org/10.1029/2006JE002735

Ferrill, D. A., Wyrick, D. Y., & Smart, K. J. (2011). Coseismic, dilational-fault and extension-fracture related pit chain formation in Iceland: Analog for pit chains on Mars. *Lithosphere*, *3*(2), 133–142. https://doi.org/10.1130/L123.1

Flahaut, J., Mustard, J. F., Quantin, C., Clenet, H., Allemand, P., & Thomas, P. (2011). Dikes of distinct composition intruded into Noachian-aged crust exposed in the walls of Valles Marineris. *Geophysical Research Letters*, *38*(15). https://doi.org/10.1029/2011GL048109

G Walter sebastianwalter, S. H., & van Gasselt, S. (n.d.). *HRSC Data Dissemination-Dynamic Queries and Data Interoperability*. Retrieved from http://maps.planet.fu-berlin.de

Gaddis, L., Anderson, J., Becker, K., Becker, T., Cook, D., Edwards, K., … Robinson, M. (1997). An Overview of the Integrated Software for Imaging Spectrometers (ISIS). *Lunar and*

Planetary Science Conference, 387. Retrieved from https://ui.adsabs.harvard.edu/abs/1997LPI....28..387G/abstract

Gendrin, A., Mangold, N., Bibring, J.-P., Langevin, Y., Gondet, B., Poulet, F., … LeMouélic, S. (2005). Sulfates in Martian layered terrains: the OMEGA/Mars Express view. *Science (New York, N.Y.), 307*(5715), 1587–1591. https://doi.org/10.1126/science.1109087

Glotch, T D, Rogers, D., & Christensen, P. R. (2005). A newly discovered hematite-rich unit in Aureum Chaos: Comparison of hematite and associated units with those in Aram Chaos. *36th Annual Lunar and Planetary Science Conference*, *36*.

Glotch, Timothy D, & Christensen, P. R. (2005). Geologic and mineralogic mapping of Aram Chaos: Evidence for a water-rich history. *Journal of Geophysical Research: Planets*, *110*(E9).

Glotch, Timothy D, & Rogers, A. D. (2007). *Evidence for aqueous deposition of hematite- and sulfate-rich light-toned layered deposits in Aureum and Iani Chaos, Mars*. https://doi.org/10.1029/2006JE002863

Hall, J. L., Solomon, S. C., & Head, J. W. (1981). Lunar floor-fractured craters: Evidence for viscous relaxation of crater topography. *Journal of Geophysical Research: Solid Earth*, *86*(B10), 9537–9552. https://doi.org/10.1029/jb086ib10p09537

Harrison, K. P., & Grimm, R. E. (2008). Multiple flooding events in Martian outflow channels. *Journal of Geophysical Research*, *113*(E2), E02002. https://doi.org/10.1029/2007JE002951

Harrison, K. P., & Grimm, R. E. (2009). Regionally compartmented groundwater flow on Mars. *Journal of Geophysical Research: Planets*, *114*(E4).

Head, J. W., & Wilson, L. (2002). Mars: a review and synthesis of general environments and geological settings of magma-H_2O interactions. *Geological Society, London, Special*

Publications, *202*(1), 27–57. https://doi.org/10.1144/GSL.SP.2002.202.01.03

Head, J. W., & Wilson, L. (2007). Heat transfer in volcano–ice interactions on Mars: synthesis of environments and implications for processes and landforms. *Annals of Glaciology, 45*, 1–13. https://doi.org/10.3189/172756407782282570

Hoffman, N. (2000). White Mars: A New Model for Mars' Surface and Atmosphere Based on CO2. *Icarus*, *146*(2), 326–342. https://doi.org/10.1006/ICAR.2000.6398

Hoke, M. R. T., Hynek, B. M., & Tucker, G. E. (2011). Formation timescales of large Martian valley networks. *Earth and Planetary Science Letters*, *312*(1–2), 1–12. https://doi.org/10.1016/j.epsl.2011.09.053

Inoue, A.; Utada, M.; Nagata, U.; Watanabe, T. (1984). Conversion of trioctahedral smectite to interstratified Chlorite/Smectite in Pliocene acidic pyroclastic sediments of the Ohyu district, Akita Prefecture, Japan. *Clay Science*, *6*(3), 103–116. https://doi.org/10.11362/jcssjclayscience1960.6.103

Inoue, A. (1995). Formation of Clay Minerals in Hydrothermal Environments. In *Origin and Mineralogy of Clays* (pp. 268–329). https://doi.org/10.1007/978-3-662-12648-6_7

Irwin, R. P., Tooth, S., Craddock, R. A., Howard, A. D., & De Latour, A. B. (2014). Origin and development of theater-headed valleys in the atacama desert, northern chile: Morphological analogs to martian valley networks. *Icarus*, *243*, 296–310. https://doi.org/10.1016/j.icarus.2014.08.012

Jaeger, W. L., Keszthelyi, L. P., Skinner, J. A., Milazzo, M. P., McEwen, A. S., Titus, T. N., … Kirk, R. L. (2010). Emplacement of the youngest flood lava on Mars: A short, turbulent story. *Icarus*, *205*(1), 230–243. https://doi.org/10.1016/j.icarus.2009.09.011

Jakosky, B. M., Mellon, M. T., Kieffer, H. H., Christensen, P. R., Varnes, E. S., & Lee, S. W. (2000). The thermal inertia of Mars from the Mars Global Surveyor Thermal Emission Spectrometer. *Journal of Geophysical Research: Planets*, *105*(E4), 9643–9652. https://doi.org/10.1029/1999JE001088

Jozwiak, L. M., Head, J. W., & Wilson, L. (2015). Lunar floor-fractured craters as magmatic intrusions: Geometry, modes of emplacement, associated tectonic and volcanic features, and implications for gravity anomalies. *Icarus*, *248*, 424–447. https://doi.org/10.1016/j.icarus.2014.10.052

Jozwiak, L. M., Head, J. W., Zuber, M. T., Smith, D. E., & Neumann, G. A. (2012). Lunar floor-fractured craters: Classification, distribution, origin and implications for magmatism and shallow crustal structure. *Journal of Geophysical Research E: Planets*, *117*(11). https://doi.org/10.1029/2012JE004134

Kargel, J. S., Furfaro, R., Prieto-Ballesteros, O., Rodriguez, J. A. P., Montgomery, D. R., Gillespie, A. R., … Wood, S. E. (2007). Martian hydrogeology sustained by thermally insulating gas and salt hydrates. *Geology*, *35*(11), 975–978.

King, T. V. V., & Ridley, W. I. (1987). Relation of the spectroscopic reflectance of olivine to mineral chemistry and some remote sensing implications. *Journal of Geophysical Research: Solid Earth, 92*(B11), 11457–11469. https://doi.org/10.1029/JB092iB11p11457

Kneissl, T., Van Gasselt, S., Wendt, L., Gross, C., & Neukum, G. (2011). Layering and degradation of the Rupes Tenuis unit, Mars--a structural analysis south of Chasma Boreale. *Geological Society, London, Special Publications, 356*(1), 257–279.

Koeppen, W. C., & Hamilton, V. E. (2008). Global distribution, composition, and abundance of olivine on the surface of Mars from thermal infrared data. *Journal of Geophysical Research E:*

Planets, *113*(5). https://doi.org/10.1029/2007JE002984

Lamb, M. P., Howard, A. D., Johnson, J., Whipple, K. X., Dietrich, W. E., & Perron, J. T. (2006). Can springs cut canyons into rock? *Journal of Geophysical Research*, *111*(E7), E07002. https://doi.org/10.1029/2005JE002663

Le Deit, L., Le Mouélic, S., Bourgeois, O., Combe, J.-P., Mège, D., Sotin, C., … Bibring, J.-P. (2008). Ferric oxides in East Candor Chasma, Valles Marineris (Mars) inferred from analysis of OMEGA/Mars Express data: Identification and geological interpretation. *Journal of Geophysical Research*, *113*(E7), E07001. https://doi.org/10.1029/2007JE002950

Leask, H. J., Wilson, L., & Mitchell, K. L. (2006). Formation of Aromatum Chaos, Mars: Morphological development as a result of volcano-ice interactions. *Journal of Geophysical Research: Planets*, *111*(E8).

Leask, H. J., Wilson, L., & Mitchell, K. L. (2007). Formation of Mangala Valles outflow channel, Mars: Morphological development and water discharge and duration estimates. *Journal of Geophysical Research: Planets*, *112*(E8). https://doi.org/10.1029/2006JE002851

Leone, G. (2014). A network of lava tubes as the origin of Labyrinthus Noctis and Valles Marineris on Mars. *Journal of Volcanology and Geothermal Research*, *277*, 1–8.

Leverington, D. W. (2011, September 15). A volcanic origin for the outflow channels of Mars: Key evidence and major implications. *Geomorphology*, Vol. 132, pp. 51–75. https://doi.org/10.1016/j.geomorph.2011.05.022

Lichtenberg, K. A., Arvidson, R. E., Morris, R. V., Murchie, S. L., Bishop, J. L., Fernandez Remolar, D., … Roach, L. H. (2010). Stratigraphy of hydrated sulfates in the sedimentary deposits of Aram Chaos, Mars. *Journal of Geophysical Research*, *115*(E6), E00D17.

https://doi.org/10.1029/2009JE003353

Liu, Y., Arvidson, R. E., Wolff, M. J., Mellon, M. T., Catalano, J. G., Wang, A., & Bishop, J. L. (2012). Lambert albedo retrieval and analyses over Aram Chaos from OMEGA hyperspectral imaging data. *J. Geophys. Res*, *117*, 0–11. https://doi.org/10.1029/2012JE004056

Luzzi, E. R. A. P. C. C. A. F. (2020). Geological Map of Arsinoes and Pyrrhae Chaos, Mars. Retrieved June 10, 2020, from https://data.4tu.nl/repository/uuid:c4b7c436-5af3-449f-9757-908ca5a73258/object/citation

Malin, M. C., Bell, J. F., Cantor, B. A., Caplinger, M. A., Calvin, W. M., Clancy, R. T., … Wolff, M. J. (2007). Context Camera Investigation on board the Mars Reconnaissance Orbiter. *Journal of Geophysical Research: Planets*, *112*(E5).

Manker, J. P., & Johnson, A. P. (1982). Simulation of Martian chaotic terrain and outflow channels. *Icarus*, *51*(1), 121–132. https://doi.org/10.1016/0019-1035(82)90032-X

Massé, M., Mouélic, S. Le, Bourgeois, O., Combe, J.-P., Deit, L. Le, Sotin, C., … Langevin, Y. (2008). Mineralogical composition, structure, morphology, and geological history of Aram Chaos crater fill on Mars derived from OMEGA Mars Express data. *J. Geophys. Res*, *113*, 12006. https://doi.org/10.1029/2008JE003131

McEwen, A. S., Eliason, E. M., Bergstrom, J. W., Bridges, N. T., Hansen, C. J., Delamere, W. A., … Weitz, C. M. (2007). MRO's High Resolution Imaging Science Experiment (HiRISE). *Journal of Geophysical Research: Planets*, *112*(E5).

Mège, D., & Gurgurewicz, J. (2016). On Mars, Location and Orientation of Dykes Exposed along the Valles Marineris Walls Reveal Expected and Unexpected Stress Fields. *Acta Geologica Sinica - English Edition*, *90*(s1), 177–179. https://doi.org/10.1111/1755-6724.12959

Mège, D., & Masson, P. (1996). Amounts of crustal stretching in Valles Marineris, Mars. In *Plmet. Space Sci* (Vol. 44).

Mellon, M. T., Jakosky, B. M., Kieffer, H. H., & Christensen, P. R. (2000). High-Resolution Thermal Inertia Mapping from the Mars Global Surveyor Thermal Emission Spectrometer. *Icarus*, *148*, 437–455. https://doi.org/10.1006/icar.2000.6503

Meresse, S., Costard, F., Mangold, N., Masson, P., Neukum, G., & others. (2008). Formation and evolution of the chaotic terrains by subsidence and magmatism: Hydraotes Chaos, Mars. *Icarus*, *194*(2), 487–500.

Montési, L. G. J. (2001). Concentric dikes on the flanks of Pavonis Mons: Implications for the evolution of martian shield volcanoes and mantle plumes. *Special Paper of the Geological Society of America*, *352*, 165–181. https://doi.org/10.1130/0-8137-2352-3.165

Moratto, Z. M., Broxton, M. J., Beyer, R. A., Lundy, M., & Husmann, K. (2010). Ames Stereo Pipeline, NASA's open source automated stereogrammetry software. *Lunar and Planetary Science Conference*, *41*, 2364.

Mouginis-Mark, P. J., & Christensen, P. R. (2005). New observations of volcanic features on Mars from the THEMIS instrument. *Journal of Geophysical Research: Planets*, *110*(E8).

Murchie, S., Arvidson, R., Bedini, P., Beisser, K., Bibring, J.-P., Bishop, J., … Wolff, M. (2007). Compact Reconnaissance Imaging Spectrometer for Mars (CRISM) on Mars Reconnaissance Orbiter (MRO). *Journal of Geophysical Research*, *112*(E5), E05S03. https://doi.org/10.1029/2006JE002682

Okubo, C. H., & Martel, S. J. (n.d.). Pit crater formation on Kilauea volcano, Hawaii. In *Journal of Volcanology and Geothermal Research* (Vol. 86).

Okubo, C. H., & Schultz, R. A. (2005). *Evidence of normal faulting and dike intrusion at Valles Marineris from pit crater topography*.

Ormö, J., Komatsu, G., Chan, M. A., Beitler, B., & Parry, W. T. (2004). Geological features indicative of processes related to the hematite formation in Meridiani Planum and Aram Chaos, Mars: a comparison with diagenetic hematite deposits in southern Utah, USA. *Icarus, 171*, 295–316. https://doi.org/10.1016/j.icarus.2004.06.001

Pozzobon, R., Mazzarini, F., Massironi, M., & Marinangeli, L. (2015). Self-similar clustering distribution of structural features on Ascraeus Mons (Mars): implications for magma chamber depth. *Geological Society, London, Special Publications, 401*(1), 203–218.

Roda, M., Kleinhans, M. G., Zegers, T. E., & Oosthoek, J. H. P. (2014). Catastrophic ice lake collapse in Aram Chaos, Mars. *Icarus, 236*, 104–121.

Rodriguez, J. A. P., Sasaki, S., Kuzmin, R. O., Dohm, J. M., Tanaka, K. L., Miyamoto, H., … Ferris, J. C. (2005). Outflow channel sources, reactivation, and chaos formation, Xanthe Terra, Mars. *Icarus, 175*(1), 36–57.

Schmidt, G., Fueten, F., Stesky, R., Flahaut, J., & Hauber, E. (2018). Geology of Hebes Chasma, Mars: 1. Structure, Stratigraphy, and Mineralogy of the Interior Layered Deposits. *Journal of Geophysical Research: Planets*, *123*(11), 2893–2919. https://doi.org/10.1029/2018JE005658

Schultz, P. H., Schultz, R. A., & Rogers, J. (1982). The structure and evolution of ancient impact basins on Mars. *Journal of Geophysical Research: Solid Earth, 87*(B12), 9803–9820.

Scott, E. D., & Wilson, L. (1999). Evidence for a sill emplacement event on the upper flanks of the Ascraeus Mons shield volcano, Mars. *Journal of Geophysical Research: Planets, 104*(E11), 27079–27089. https://doi.org/10.1029/1999JE001049

Scott, E. D., & Wilson, L. (2002). Plinian eruptions and passive collapse events as mechanisms of formation for Martian pit chain craters. *Journal of Geophysical Research E: Planets*, *107*(4), 4–1. https://doi.org/10.1029/2000je001432

Sefton-Nash, E., Catling, D. C., Wood, S. E., Grindrod, P. M., & Teanby, N. A. (2012). Topographic, spectral and thermal inertia analysis of interior layered deposits in Iani Chaos, Mars. *Icarus*, *221*(1), 20–42. https://doi.org/10.1016/j.icarus.2012.06.036

Sowe, M, Wendt, L., McGuire, P. C., & Neukum, G. (2012). Hydrated minerals in the deposits of Aureum Chaos. *Icarus*, *218*(1), 406–419.

Sowe, Mariam, Stesky, R., Fueten, F., Sowe, M., Hauber, E., Jaumann, R., … Neukum, G. (2007). LAYERED DEPOSITS OF IANI CHAOS ON MARS Interior Layered Deposits in the Eastern Valles Marineris and Chaotic Terrains on Mars. *Lunar Planet. Sci.*, *XXXVIII*. https://doi.org/10.1029/2004JE002389

Survey, U. S. G. (2006). FGDC Digital Cartographic Standard for Geologic Map Symbolization (PostScript Implementation) Prepared in cooperation with the Geologic Data Subcommittee of the\rFederal Geographic Data Committee. *U.S. Geological Survey Techniques and Methods 11-A2*.

Tanaka, K. L. & G. M. P. (1989). Martian tension fractures and the formation of grabens and collapse features at Valles Marineris. *Lunar and Planetary Science Conference, 19th, Houston, TX, Mar. 14-18, 1988, Proceedings (A89-36486 15-91)*, 383–396. Retrieved from http://articles.adsabs.harvard.edu/cgi-bin/nph-iarticle_query?bibcode=1989LPSC...19..383T&db_key=AST&page_ind=10&plate_select=NO&data_type=GIF&type=SCREEN_GIF&classic=YES

Tanaka, K. L., Robbins, S. J., Fortezzo, C. M., Skinner Jr, J. A., & Hare, T. M. (2014). The digital global geologic map of Mars: Chronostratigraphic ages, topographic and crater morphologic characteristics, and updated resurfacing history. *Planetary and Space Science*, *95*, 11–24.

Tange, O. (2011). GNU Parallel: The Command-Line Power Tool | USENIX. *The USENIX Magazine*, *3*(1), 42–47. Retrieved from https://www.usenix.org/publications/login/february-2011-volume-36-number-1/gnu-parallel-command-line-power-tool

Thorey, C., & Michaut, C. (2014). A model for the dynamics of crater-centered intrusion: Application to lunar floor-fractured craters. *Journal of Geophysical Research: Planets*, *119*(1), 286–312. https://doi.org/10.1002/2013JE004467

Viviano-Beck, C. E., Seelos, F. P., Murchie, S. L., Kahn, E. G., Seelos, K. D., Taylor, H. W., … others. (2014). Revised CRISM spectral parameters and summary products based on the currently detected mineral diversity on Mars. *Journal of Geophysical Research: Planets*, *119*(6), 1403–1431.

Wichman, R. W., & Schultz, P. H. (1996). Crater-centered laccoliths on the Moon: Modeling intrusion depth and magmatic pressure at the crater Taruntius. *Icarus*, *122*(1), 193–199. https://doi.org/10.1006/icar.1996.0118

Wilson, L., & Head III, J. W. (2002). Tharsis-radial graben systems as the surface manifestation of plume-related dike intrusion complexes: Models and implications. *Journal of Geophysical Research: Planets*, *107*(E8), 1.

Wyrick, D. (2004). Distribution, morphology, and origins of Martian pit crater chains. *Journal of Geophysical Research*, *109*(E6), E06005. https://doi.org/10.1029/2004JE002240

Zegers, T. E., Oosthoek, J. H. P., Rossi, A. P., Blom, J. K., & Schumacher, S. (2010). Melt and collapse of buried water ice: An alternative hypothesis for the formation of chaotic terrains on

Mars. *Earth and Planetary Science Letters*, *297*(3–4), 496–504.

8 Tables and captions

Fig. 1: Location of Arsinoes and Pyrrhae Chaos on a MOLA Global Color Shaded Relief.

Figure 2: Elevation contours in Pyrrhae Chaos showing the mesas of the Fractured plains at higher elevations compared the mounds of the Knobby Terrain. CTX mosaic; HRSC DEM from orbit *h1958_0000.*

Figure 3: A) Overview map of the area where the contact between the two non-disrupted units occurs. The black square bounds the area depicted in D. The section X-X' refers to the topographic profile in C. B) 3D view of the stratigraphic contact between the Light-toned Layered Unit and the Cap Unit, separated by the unconformity (in blue). C) Topographic profile showing the plateau-like morphology of the Cap Unit and the different attitude of the units. D) Some of the attitudes measured with LayerTools (light blue: Light-toned Layered Unit; black: Cap Unit). CTX stereo pair: *B05_011700_1720_XI_08S028W* and *B06_012056_1721_XI_07S028W*.

Figure 4: The light-toned layered deposits overlying the Knobby Terrain and outflanking the mounds (black arrows). The superposition relationships suggest a younger age of the layered deposits relatively to the knobs. Note also the tendency to assume a lobate morphology. CTX: *F10_039563_1729_XN_07S027W.*

Figure 5: Faults and the elongated graben-like depressions mapped in red in Arsinoes Chaos (A) and Pyrrhae Chaos (B). The locations of Fig. 5 B-C-D and Fig. 9 are indicated in Fig. 5A. C) The elongated graben-like depressions occur close to the faults affecting the Fractured Plains and it is difficult to distinguish their separation. D) The elongated graben-like depressions are also coalescent with pit chain (black arrows) and are often associated with heavily pitted areas (pink area). CTX mosaic.

Figure 6: Two wrinkle ridges are indicated by the black arrows. CTX mosaic.

Figure 7: Topographic profiles of the northeastern (top) and southeastern (bottom) craters. The images for context are from the CTX mosaic, the DEM used for the profiles is a MOLA-HRSC blended DEM.

Fig. 8: Contact between the younger lava flow and the underlying basalts, both cut by collapse-related faults. HiRISE image ESP_037123_1690 (black & white in A and C, false color in B.

Figure 9: A) 3D view of the false colour HRSC image *h1947_0000*, showing a difference in tone between the Fractured Plains materials and the lava flow indicated by the white arrow. The black arrow points to a y-shaped conjunction within an elongated graben-like depression in the south-eastern Pyrrhae Chaos. B) The same features displayed in A are now showed in another perspective

and in THEMIS-Derived Global Thermal Inertia Mosaic. Note that the lava flow occurring in Pyrrhae Chaos (white arrow) has a higher thermal inertia than the surrounding materials.

Figure 10: **A)** Location of the CRISM *cube frt00008233_07* superposed on the geomorphic map where the different units are shown. The complete geomorphic map with legend is presented in Fig. 15. **B)** True colors image (R=R600; G=R530; B=R440). **C)** RGB composite with summary parameters of the CRISM TRDR *frt00008233* scene. CHL: Chlorides are in blue, yellow/green are indicative of hydrated minerals (R= ISLOPE; G= BD3000; B=IRR2).

Figure 11: Location of the peripheral CRISM cubes *frt00023790_07 and frt000196b0_07* on the CTX mosaic.

Figure 12: A) Infrared false color scene showing a mineralogical variation between the exhumed deposits and the surrounding bedrock. B) RGB composite with summary products for phyllosilicates with Fe and Mg (PFM: cyan colors, coinciding with the albedo variation, indicate Fe/Mg smectites, R=BD2355; G=D2300; B=BD2290). C) The band depth at 2.3 μm is significant in correspondence of the hydrated minerals. On the right, the ratioed spectrum is compared to resampled CRISM spectra of Smectite 397S170, Illite LAIL01, and Hisingerite LAHI01 from the spectral library. The black lines highlight the absorptions of the ratioed spectrum at 1.42, 1.92 and 2.28 μm. CRISM cube *frt000196b0_07*.

Figure 13: A) LCPINDEX shows the abundances of pyroxenes on the bedrock. B) Interpretation of the mineralogical variation: in the central region the hydrated minerals are interpreted as Fe-Mg phyllosilicates (smectite), while the bedrock rich in pyroxenes is indicative of basaltic compositions. CRISM cube *frt000196b0_07*.

Figure 14: A) False color scene and location of s1 and s2; B) the ratioed spectrum is compared to the CRISM resampled spectra for clinopyroxene C1PP4 and orthopyroxene CBSB51. Both the absorption at 1 μm and the broad absorption at 2 μm are present and consistent with a mafic composition.

CRISM cube *frt00023790_07*.

Figure 15: Morpho-stratigraphic map of Arsinoes and Pyrrhae Chaos.

Table 1: List of images and data cubes used in this work.

Dataset	Image ID	Stereo pair
HiRISE	ESP_016658_1735	-
HiRISE	ESP_020060_1715	-

HiRISE	ESP_026996_1725	-
HiRISE	ESP_027629_1730	-
HiRISE	ESP_034499_1710	-
HiRISE	ESP_035356_1715	-
HiRISE	ESP_036622_1720	-
HiRISE	ESP_037545_1730	-
HiRISE	ESP_039352_1730	-
HiRISE	ESP_053883_1730	-
HiRISE	PSP_002180_1720	-
HiRISE	ESP_037123_1690	-
CTX	B05_011700_1720_XI_08S028W	B06_012056_1721_XI_07S028W
CTX	F10_039563_1729_XN_07S027W	P04_002747_1736_XN_06S027W
CRISM	frt00008233_07	-
CRISM	frt00023790_07	-
CRISM	frt000196b0_07	-
HRSC	h1947_0000	-
HRSC	h1958_0000	